Published in final edited form as:

Cell Rep. 2024 July 23; 43(7): 114492. doi:10.1016/j.celrep.2024.114492.

The polySUMOylation axis promotes nucleolar release of Tof2 for mitotic exit

Emily Gutierrez-Morton[1], **Cory Haluska**[2], **Liam Collins**[3], **Raed Rizkallah**[1], **Robert J. Tomko Jr.**[1], **Yanchang Wang**[1,4,*]

[1]Department of Biomedical Sciences, College of Medicine, Florida State University, Tallahassee, FL 32306, USA

[2]Molecular Biology Program, Memorial Sloan Kettering Cancer Center, New York, NY 10065, USA

[3]College of Arts and Sciences, Florida State University, Tallahassee, FL 32306, USA

[4]Lead contact

SUMMARY

In budding yeast, the nucleolus serves as the site to sequester Cdc14, a phosphatase essential for mitotic exit. Nucleolar proteins Tof2, Net1, and Fob1 are required for this sequestration. Although it is known that these nucleolar proteins are SUMOylated, how SUMOylation regulates their activity remains unknown. Here, we show that Tof2 exhibits cell-cycle-regulated nucleolar delocalization and turnover. Depletion of the nuclear small ubiquitin-like modifier (SUMO) protease Ulp2 not only causes Tof2 polySUMOylation, nucleolar delocalization, and degradation but also leads to Cdc14 nucleolar release and activation. This outcome depends on polySUMOylation and the activity of downstream enzymes, including SUMO-targeted ubiquitin ligase and Cdc48/p97 segregase. We further developed a system to tether SUMO machinery to Tof2 and generated a SUMO-deficient *tof2* mutant, and the results indicate that Tof2 polySUMOylation is necessary and sufficient for its nucleolar delocalization and degradation. Together, our work reveals a polySUMO-dependent mechanism that delocalizes Tof2 from the nucleolus to facilitate mitotic exit.

Graphical Abstract

*Correspondence: yanchang.wang@med.fsu.edu.

AUTHOR CONTRIBUTIONS

Conceptualization, Y.W., E.G.-M., and R.J.T.; methodology, E.G.-M. and Y.W.; investigation, E.G.-M., C.H., L.C., R.R., and Y.W.; Writing – original draft, E.G.-M. and Y.W.; writing – review and editing, E.G.-M., Y.W., and R.J.T.; funding acquisition, Y.W., R.J.T., and R.R.; supervision, Y.W. and R.J.T.

SUPPLEMENTAL INFORMATION

Supplemental information can be found online at https://doi.org/10.1016/j.celrep.2024.114492.

DECLARATION OF INTERESTS

The authors declare no competing interests.

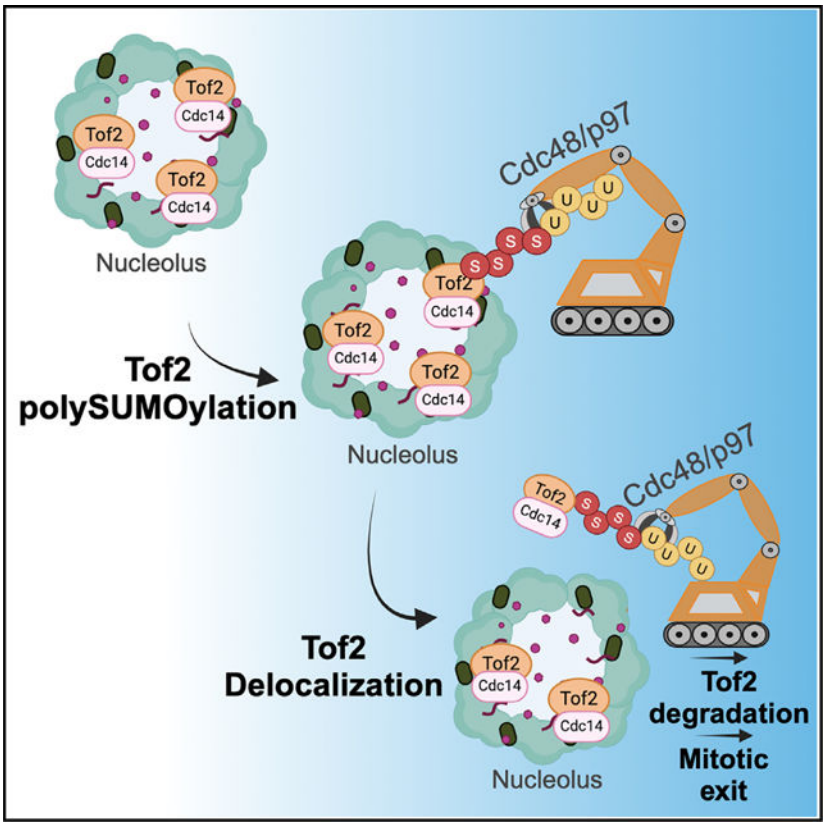

In brief

Gutierrez-Morton et al. demonstrate cell-cycle-regulated nucleolar localization and protein abundance of Tof2, a SUMO substrate that anchors Cdc14 phosphatase to the nucleolus. Tof2 polySUMOylation triggers its ubiquitination by STUbL, extraction by Cdc48, and degradation by the proteasome, which promotes the nucleolar release of Cdc14 for mitotic exit.

INTRODUCTION

SUMOylation attaches a small ubiquitin-like modifier (SUMO) to target proteins, which controls protein subcellular localization, abundance, and function.[1] In the budding yeast *S. cerevisiae*, more than 100 SUMO substrates have been identified.[2,3] Human cells have about 7,000 SUMO proteins, and perturbations to SUMO homeostasis are correlated with cancers and neurodegenerative diseases.[4,5] Similar to ubiquitination, SUMOylation is catalyzed through a sequential cascade involving an E1 activating enzyme, an E2 conjugating enzyme, and E3 SUMO ligases.[6,7] Budding yeast contains heterodimer, Aos1/Uba2, as SUMO E1; a single E2, Ubc9; and several E3 ligases, including Siz1, Siz2, Mms21, and Zip3.[8–10] In contrast, SUMO proteases remove SUMO moieties from SUMO substrates. The two SUMO proteases in budding yeast are Ulp1 and Ulp2. Although both recognize nuclear substrates, Ulp1 is responsible for the maturation of SUMO, whereas Ulp2 plays a major role in cleaving polySUMO chains.[11–13]

A protein can be modified by monoSUMOylation or polySUMOylation.[14] MonoSUMOylation promotes formation of biomolecular condensates or macromolecular complexes through the interaction between SUMO and SUMO-interacting motifs (SIMs).[15,16] In contrast, polySUMOylation aids in macromolecular complex disassembly by triggering downstream events. SUMO-targeted ubiquitin ligases (STUbLs) selectively recognize SUMO chains, ubiquitinating the SUMOylated substrates. The best studied STUbL in budding yeast is the Slx5/Slx8 heterodimer.[17–19] Substrate ubiquitination by STUbL enables extraction by segregase Cdc48/p97/VCP (valosin-containing protein) for proteasomal destruction.[20,21] Interestingly, monoSUMOylation can also drive relocalization of damaged DNA and stalled replication forks.[22,23] This study focuses on the role of a polySUMO-dependent pathway in protein relocation.

The SUMO proteins in budding yeast are enriched in several cell-cycle-related protein complexes, including the regulator of nucleolar silencing and telophase exit (RENT) complex, which localizes within the nucleolus.[2,3] Among the RENT proteins, Fob1, Tof2, and Net1/Cfi1 are SUMO substrates.[3,24] Fob1 binds to rDNA and further recruits Tof2 and Net1, whereas Net1 also associates with rDNA in Fob1-independent manners.[25,26] Tof2 and Net1 function as the nucleolar anchors for Cdc14 phosphatase, which antagonizes cyclin-dependent kinase (CDK) to enable mitotic exit.[27] Prior to anaphase onset, Cdc14 is sequestered within the nucleolus, which prevents its access to CDK substrates.[28–30] The bi-phasic nucleolar release of Cdc14 is dictated by two mitotic exit pathways, Cdc14 early anaphase release (FEAR) and mitotic exit network (MEN). FEAR promotes a brief Cdc14 release in early anaphase, and MEN activation leads to robust Cdc14 release in late anaphase.[31] Once released, Cdc14 phosphatase reverses CDK-imposed phosphorylation and facilitates anaphase progression.[32,33] Mitotic CDK phosphorylates Net1 to trigger its Cdc14 release,[34–36] but how cells regulate Cdc14 release from Tof2 remains largely enigmatic.

In this study, we investigated how polySUMOylation of the yeast RENT proteins Tof2/Net1/Fob1 controls Cdc14 release. We first showed that the abundance of polySUMO conjugates was cell cycle regulated. Interestingly, Tof2, but not Net1 and Fob1, exhibited reduced nucleolar localization and proteasomal degradation after anaphase onset. We further uncovered that induction of polySUMOylation by nuclear depletion of SUMO protease Ulp2 caused untimely nucleolar delocalization and degradation of Tof2 as well as premature mitotic exit. Inhibiting STUbL or Cdc48 activity suppressed polySUMO-induced Tof2 delocalization and degradation, suggesting the role of the polySUMO axis in this process. We further showed that chemical-genetic modulation of Tof2 SUMOylation was sufficient to control its nucleolar delocalization and degradation. Finally, a SUMO-deficient Tof2 mutant protein showed resistance to polySUMO-induced Tof2 nucleolar delocalization and degradation. Altogether, these findings support the conclusion that the polySUMO axis promotes delocalization and degradation of the nucleolar protein Tof2 to facilitate mitotic exit.

RESULTS

PolySUMOylation is cell-cycle regulated and critical for mitotic progression

SUMOylation is critical for DNA replication and mitotic progression.[37,38] Thus, the level of SUMOylation may be regulated during the cell cycle. *SMT3* encodes the only SUMO in budding yeast. Using a chromosomally expressed His-FLAG-Smt3 (HF-Smt3) yeast allele,[39] we measured polySUMOylation in synchronized cells (Figure 1A). PolySUMOylation significantly increases the molecular weight of substrates, and high-molecular-weight (HMW) proteins are retained in the stacking gel due to their size. In wild-type (WT) cells, the level of HMW protein species conjugated with HF-Smt3 increased significantly 40 min after G_1 release and declined markedly at 80 min. The decline occurred simultaneously with Pds1 degradation, which marks anaphase entry.[40] Strikingly, the SUMO protease mutant *ulp2Δ*, wherein polySUMO conjugates accumulate,[41] showed a much higher level of HMW HF-Smt3 conjugates throughout the cell cycle (Figure 1A). In addition, *ulp2Δ* cells showed a cell cycle delay, as evidenced by Pds1 accumulation, suggesting that untimely polySUMOylation impairs cell cycle progression. Therefore, our results reveal cell-cycle-regulated polySUMOylation.

We next assessed the role of polySUMOylation in mitotic exit, which is marked by Cdc14 phosphatase activation. Cdc14 dephosphorylates the CDK substrate Fin1 to allow its kinetochore (KT) binding; thus, Fin1 KT localization reports on Cdc14 activation.[42,43] In Figure 1B, we analyzed the colocalization of Fin1-GFP with the KT protein Nuf2-mCherry in WT and *ulp2Δ* cells in *cdc13-1* mutants, which arrest at pre-anaphase at high temperature due to DNA damage checkpoint activation.[44] After 2-h incubation at 36°C to achieve pre-anaphase arrest, most *cdc13-1* cells (99%) showed undetectable Fin1 KT localization. Interestingly, 33% of *cdc13-1 ulp2Δ* cells exhibited Fin1 KT localization, suggesting Cdc14 activation. To test whether polySUMOylation is required for Cdc14 activation in *cdc13-1 ulp2Δ* cells, we utilized a yeast SUMO mutant in which all lysine residues in SUMO (Smt3) were mutated to arginine (*smt3-KRall*) to block SUMO chain formation.[37,45] The introduction of the *smt3-KRall* mutant abolished premature Fin1 KT localization in *cdc13-1 ulp2Δ* cells (2%).

We also examined the role of polySUMOylation in mitotic exit using *cdc15-2* arrested telophase cells, where Cdc14 release relies solely on FEAR.[31] After 2-h incubation at 36°C, most *cdc15-2* cells showed elongated spindles, with 98% exhibiting KT-localized Fin1, indicating Cdc14 activation (Figure 1C). Slk19 is a FEAR component, and *slk19Δ* blocks Cdc14 activation in *cdc15-2* cells.[31] In *slk19Δ cdc15-2* cells, the cells with Fin1 KT localization decreased to 31%. Like *slk19Δ*, *smt3-KRall* also reduced the frequency of Fin1 KT localization (71%), indicating the role of polySUMOylation in Cdc14 activation. Additionally, *smt3-KRall* cells exhibited slowed growth and cell cycle delay, along with compromised Pds1 degradation and increased abnormal spindle frequency (Figures S1A–S1C). These results suggest the mitotic, albeit non-essential, role of polySUMOylation.

The localization and abundance of Tof2, a nucleolar anchor for Cdc14, is cell-cycle regulated

Cdc14 localizes within the nucleolus by associating with the anchor proteins Net1 and Tof2 until anaphase entry.[28–30] Fob1 recruits Tof2 and some Net1 to rDNA.[25,26] We monitored Net1, Tof2, and Fob1 localization and levels throughout the cell cycle. Net1-GFP and Fob1-GFP fluorescence remained steady after G_1 release (Figures 2A and 2B). However, Tof2-GFP showed an initial increase at 60 min, followed by a decline at 80 min, indicating Tof2 delocalization and/or degradation. Live-cell imaging during nuclear separation revealed stable Net1-GFP signal but decreased Tof2-GFP as the nucleus divided (Figure S2A), suggesting distinct regulation of Tof2 and Net1. Western blotting confirmed cell-cycle-regulated levels of Tof2 but not Fob1 and Net1 (Figure 2C). We also noticed that Tof2-GFP peaked at 60 min after G_1 release, but Tof2-myc peaked at 80 min. This difference may stem from slight variations in cell-cycle kinetics or nucleolar signal loss preceding degradation.

The release of Cdc14 from the nucleolus is controlled by two mitotic exit pathways, FEAR and MEN.[32] We further investigated if Tof2 delocalization was controlled by these mitotic pathways. Yeast mutants deficient for MEN (*cdc15-2*) and mutants deficient for both MEN and FEAR (*cdc15-2 slk19Δ* and *cdc15-2 spo12Δ*) were used to examine Tof2 localization.[31] Following G_1 release into 37°C medium to inactivate Cdc15, WT and *cdc15-2* mutant cells showed a significant decrease in Tof2-GFP intensity after anaphase entry (Figure S2B), suggesting that MEN is dispensable for Tof2 relocalization/degradation. However, in *cdc15-2 slk19Δ* and *cdc15-2 spo12Δ* cells, a persistent Tof2-GFP signal was detected. Therefore, Tof2 relocalization/degradation likely depends on the activation of FEAR but not MEN.

As a nucleolar anchor for Cdc14, the role of Tof2 in regulating Cdc14 activity remains controversial.[30,46] Therefore, we examined the effect of *TOF2* deletion on both nucleolar localization and activity of Cdc14. In *cdc13-1* arrested cells, both MEN and FEAR are inactive.[44] We used KT localization of Fin1 protein to monitor Cdc14 activation. As shown in Figure 2D, after G_1 release of *cdc13-1* cells for 140 min at 34°C, few cells showed Fin1 KT localization (5%). However, 78% of *cdc13-1 tof2*Δ cells showed Fin1-GFP KT localization, indicating Cdc14 activation. We also examined nucleolar localization of Cdc14 in *cdc13-1* and *cdc13-1 tof2Δ* cells using Nop1 as a nucleolar marker. In *cdc13-1* arrested cells, the majority of Cdc14-GFP signal colocalized with Nop1-mApple (Figure S2C). In contrast, the Cdc14-GFP signal colocalized with Nop1 decreased in *cdc13-1 tof2Δ* cells. Additionally, many *cdc13-1 tof2Δ* cells showed speckled GFP outside the nucleolus, suggesting that the absence of Tof2 triggers partial Cdc14 release.

Tof2 undergoes a polySUMO-dependent relocalization and turnover during the cell cycle

Because Tof2 is a SUMO substrate, SUMOylation may contribute to cell-cycle-regulated Tof2 nucleolar localization and degradation. We examined Tof2 protein levels during the cell cycle in different SUMO mutants, including SUMO protease mutants *ulp2Δ* with upregulated polySUMOylation,[47] *smt3-KRall* mutants showing abolished SUMO chain formation,[45] and STUbL mutants *slx5Δ* lacking polySUMO-targeted ubiquitination.[17] G_1-

arrested WT, *ulp2Δ*, *smt3-KRall*, *ulp2Δ smt3-KRall*, and *slx5Δ* cells expressing Tof2-13myc were released into the cell cycle. Consistently, Tof2 levels peaked 80 min following G_1 release in WT cells (Figure 3A). In *ulp2Δ* cells, however, Tof2 levels decreased significantly, and upshifted Tof2 bands were visible throughout the cell cycle, a likely result of polySUMOylation (Figures 3A and S2D). Conversely, the Tof2 level was relatively abundant in *smt3-KRall*, *ulp2Δ smt3-KRall*, and *slx5Δ* cells, with impaired Tof2 turnover at late time points during the cell cycle. These results support the notion that upregulated polySUMOylation destabilizes Tof2, but abolished polySUMOylation or polySUMO-targeted ubiquitination stabilizes Tof2.

We further used live-cell imaging to examine Tof2-GFP localization and intensity during nuclear separation in WT and SUMO mutants (Figures 3B and 3C). In *smt3-KRall* and *slx5Δ* mutant cells, Tof2-GFP intensity persisted and was higher than that in WT cells after nuclear division (Figure 3D). Interestingly, *smt3-KRall* and *slx5Δ* mutants showed a significant delay in Tof2-GFP separation relative to nuclear division (H2A-mApple), indicating impaired nucleolar separation (Figure 3E). Since FEAR-dependent Cdc14 release is required for nucleolar separation,[48,49] this result supports the conclusion that polySUMOylation promotes Tof2 degradation as well as FEAR-mediated Cdc14 release and nucleolar separation.

Recent studies indicate the role of SUMOylation in biomolecular condensate formation.[15] Given that the nucleolus is a well-characterized condensate,[50] Tof2 SUMOylation may contribute to its nucleolar localization. Because the SUMO2 E2 enzyme Ubc9 is essential, we assessed the localization of Tof2 in a temperature-sensitive mutant, *ubc9-10*.[51] Tof2 nucleolar localization was not impacted in *ubc9-10* cells incubated at 37°C (Figure S3A). Cells with depleted Ubc9 using the auxin inducible degron also showed efficient nucleolar localization of Tof2, indicating that SUMOylation is dispensable for the nucleolar localization of Tof2.

We next investigated which SUMO E3 ligase mediates Tof2 SUMOylation. In budding yeast, Siz1, Siz2, and Mms21 are the mitotic SUMO E3 ligases, whereas Zip3 is meiosis specific.[52] Because *ulp2Δ* mutants showed decreased Tof2 levels, likely due to upregulated Tof2 polySUMOylation and degradation (Figure 3A), we examined Tof2 protein levels in WT, *ulp2Δ*, *ulp2Δ siz1Δ*, *ulp2Δ siz2Δ*, and *ulp2Δ mms21-11* mutants (Figure S3B). Interestingly, *ulp2Δ siz2Δ* and *ulp2Δ mms21-11* cells, but not *ulp2Δ siz1Δ* mutants, restored Tof2 levels, indicating that Siz2 and Mms21 catalyze Tof2 SUMOylation. In support of this notion, previous studies report that Tof2 SUMOylation is mediated by Siz2 and Mms21, respectively.[3,53]

Nuclear depletion of the SUMO protease Ulp2 triggers Tof2 polySUMOylation and degradation

We observed increased protein polySUMOylation in *ulp2Δ* cells, but this mutant exhibits various phenotypes, like aneuploidy, temperature sensitivity, and growth defects, which complicates data interpretation.[41,54,55] To overcome this, we employed the “anchor away” system to conditionally remove Ulp2 from the nucleus and induce polySUMOylation.[56] This involved fusing Ulp2 with the FKBP12-rapamycin-binding (FRB) domain of human

mTOR and expressing Rpl13A (“anchor”) fused to FKBP12, allowing rapamycin-induced Ulp2 translocation from the nucleus to the cytoplasm (Figure 4A). After confirming the expression of Ulp2-FRB-GFP in Ulp2-”anchor away” (*ulp2-AA*) cells (Figure 4B), we found that *ulp2-AA* cells grew poorly in rapamycin plates (Figure S4A), similar to *ulp2Δ* cells.[57] We also confirmed nuclear depletion of Ulp2-GFP in *ulp2-AA* cells after rapamycin addition (Figure 4C). Therefore, we constructed *ulp2-AA* strains that enable conditional nuclear depletion of Ulp2 for polySUMOylation induction.

Using *ulp2-AA* strains, we first examined the effect of Ulp2 nuclear depletion on Tof2 polySUMOylation and degradation. To exclude the potential effect of cell cycle progression, we performed the experiment in cells arrested in S-phase with hydroxyurea (HU), a DNA synthesis inhibitor. To assess Tof2 SUMOylation, cell extracts from *ulp2-AA* cells expressing HFSmt3 and Tof2-13myc were immunoprecipitated (IPed) with anti-FLAG antibody for SUMOylated protein species. As expected, minimal Tof2 SUMOylation was detected in G_1 and HU-arrested cells (Figure 4D). After treating HU-arrested *ulp2-AA* cells with rapamycin to induce Ulp2 nuclear depletion, we observed increased accumulation of polySUMOylated protein species, as evidenced by the enhanced HF-Smt3 conjugates in the stacking gel after immunoprecipitation (IP). Increased Tof2 polySUMOylation was also detected. Notably, total Tof2 levels decreased after rapamycin addition, indicating Tof2 turnover. We further analyzed the effect of nuclear depletion of Ulp2 on nucleolar Tof2-GFP intensity in HU-arrested *ulp2-AA* cells (Figure 4E). After rapamycin addition for 20 min, only a faint Tof2 fluorescence signal was detected, and a nearly complete loss was noticed after 60 min, suggesting that Ulp2 nuclear depletion causes loss of Tof2-GFP intensity from the nucleolus. Similar results were obtained in nocodazole-arrested *ulp2-AA* cells after rapamycin addition (Figure S4B). In clear contrast to Tof2, the Net1-GFP signal was stable when treated with rapamycin in HU-arrested *ulp2-AA* cells (Figure S4C). Likewise, the Net1-9myc protein level was minimally affected by Ulp2 depletion (Figure S4D). Together, our findings reveal that induction of unscheduled polySUMOylation by nuclear depletion of Ulp2 triggers Tof2 polySUMOylation, loss of Tof2-GFP signal intensity, and Tof2 degradation.

Because Tof2 is a nucleolar anchor of Cdc14, we tested whether polySUMOylation induction causes Cdc14 release and activation. We constructed *cdc13-1 CDC14-GFP* and *cdc13-1 ulp2-AA CDC14-GFP* strains, which arrest at pre-anaphase at high temperatures. After incubating at 34°C for 2 h, we treated cells with rapamycin and examined the Cdc14-GFP signal (Figure S5A, top). *cdc13-1* cells showed the expected nucleolar localization of Cdc14 after rapamycin treatment, but *cdc13-1 ulp2-AA* cells exhibited dispersed Cdc14-GFP, which is characteristic of Cdc14 release. However, total Cdc14 protein levels were not affected under rapamycin treatment (Figure S5A, bottom). To test whether Cdc14 is also active, we examined Fin1 KT localization in *cdc13-1* and *cdc13-1 ulp2-AA* mutants following rapamycin treatment (Figure S5B). Almost no *cdc13-1* cells exhibited Fin1-GFP foci, indicating inactive Cdc14. In contrast, two clear Fin1-GFP foci were observed in 47% of *cdc13-1 ulp2-AA* cells, providing compelling evidence that polySUMOylation triggers Cdc14 nucleolar release and activation.

SUMO chain formation and STUbL activity are required for Tof2 chromatin dissociation and degradation triggered by Ulp2 depletion

As a nucleolar protein, Tof2 associates with chromatin at the rDNA region.[26,58,59] To examine how polySUMOylation affects Tof2 chromatin association and degradation, we performed chromatin fractionation in HU-arrested *ulp2-AA* cells treated with rapamycin.[60,61] As expected, cells arrested with HU exhibited abundant Tof2 protein level (Figure 5A). However, both total and chromatin-bound Tof2 protein levels reduced over time following rapamycin-induced Ulp2 nuclear depletion. Notably, Tof2 protein levels in the chromatin-free fraction were also reduced in rapamycin-treated cells. As conrols, the protein levels of chromatin-bound histone H3 and cytoplasmic Pgk1 remained consistent. Therefore, induction of polySUMOylation likely triggers chromatin dissociation and degradation of Tof2.

We next examined the role of polySUMOylation and STUbL in Tof2 degradation. In budding yeast, the Slx5/Slx8 heterodimer constitutes the STUbL, which ubiquitinates polySUMO substrates for degradation.[17–19] In HU-arrested *ulp2-AA* cells, significant Tof2 degradation was detected after rapamycin addition, but this degradation was blocked in SUMO chain-deficient *ulp2-AA smt3-KRall* cells and STUbL-deficient *ulp2-AA slx5Δ* cells (Figure 5B). We further examined the role of polySUMOylation and STUbL in Tof2 localization in HU-arrested *ulp2-AA* cells. Similarly, the decrease in Tof2-GFP intensity induced by nuclear depletion of Ulp2 was also blocked by *smt3-KRall* and *slx5Δ* (Figure 5C). Therefore, polySUMO chain formation and STUbL activity are essential for Tof2 chromatin dissociation and degradation.

The distinct roles of the proteasome and Cdc48 segregase in polySUMO-induced Tof2 delocalization and degradation

To test if polySUMO-induced Tof2 degradation depends on the proteasome, we used a *cim3-1* mutant, wherein the proteasomal subunit Rpt6 becomes inactive at elevated temperatures.[62] *ulp2-AA* and *cim3-1 ulp2-AA* cells with Tof2-13myc were arrested with HU at 34°C for 2 h, and then rapamycin was added to permit polySUMOylation via Ulp2 nuclear depletion (Figure 6A). The total Tof2 level was indeed stabilized in *cim3-1* cells, indicating the essential role of the proteasome in Tof2 degradation. Interestingly, we observed reduced Tof2 occupancy on chromatin as well as enriched Tof2 in the chromatin-free fraction, implying that Tof2 dissociates from chromatin before degradation. To further assess if polySUMOylation triggers Tof2 dissociation from rDNA, we performed chromatin IP (ChIP) to detect direct Tof2-rDNA association. *cim3-1 ulp2-AA TOF2-13myc* cells were arrested with HU at 36°C, and then rapamycin was added to induce polySUMOylation. Sheared DNA was recovered from cross-linked and IPed samples with anti-Myc antibody. Then, the levels of rDNA and control DNA (*CUP1*) that bound to Tof2-13myc were measured by PCR using previously designed primer pairs.[26] Strikingly, Tof2-13myc lost much of its rDNA association following polySUMOylation induction (Figure 6B). These results indicate that Tof2 polySUMOylation induces its rDNA dissociation, but Tof2 degradation is dispensable for this process.

Following SUMOylation and STUbL-mediated ubiquitination, the Cdc48 complex segregates substrates to facilitate proteasomal degradation.[20] In *cdc48-3 ulp2-AA* mutants, we observed stabilized total Tof2 and elevated Tof2 levels in the chromatin fraction after Ulp2 depletion (Figure 6A), indicating that Cdc48 is required for both chromatin dissociation and degradation of Tof2. Further investigation into Tof2 nucleolar localization revealed that *cdc48-3* mutation restored the Tof2-GFP signal at the nucleolus after polySUMOylation induction in *ulp2-AA* cells (Figure 6C). Interestingly, *cim3-1 ulp2-AA* cells showed a reduced but not abolished Tof2-GFP signal at the nucleolus, possibly due to Tof2 proteins remaining close to chromatin even after dissociation in *cim3-1* cells.

Cdc48 together with its co-factor Ufd1 recognizes SUMO-modified substrates for protein extraction, and Ufd1 harbors an SIM to mediate interaction between the Cdc48 complex and SUMO substrates.[20,63,64] To test if the SIM of Ufd1 is required for polySUMO-mediated Tof2 degradation, we examined Tof2 levels in *ulp2-AA ufd1*$^{\Delta SIM}$ cells (Figure S6A). After addition of rapamycin in HU-arrested *ulp2-AA ufd1*$^{\Delta SIM}$ cells, Tof2 turnover was compromised significantly. Additionally, polySUMO-induced Tof2-GFP delocalization was also suppressed in *ulp2-AA ufd1*$^{\Delta SIM}$ cells (Figure S6B). We further examined Cdc14 activity in *cdc15-2* and *cdc15-2 ufd1*$^{\Delta SIM}$ cells (Figure S6C). After 2-h incubation at 36°C, most *cdc15-2* cells (97%) showed KT-localized Fin1, but this number was reduced to 46% in *cdc15-2 ufd1*$^{\Delta SIM}$ mutants. Similarly, only 52% of *cdc15-2 slx5Δ* cells showed Fin1 KT localization. Taken together, these results suggest that polySUMOylation triggers Tof2 nucleolar delocalization and degradation, which subsequently causes Cdc14 nucleolar release and activation. In addition, this process requires STUbL activity and SIM-dependent recruitment of the Cdc48 complex to polySUMO substrates.

Establishing a system to tether SUMO machinery to Tof2

Depleting Ulp2 or using *smt3-KRall* alters overall SUMOylation patterns, complicating data interpretation due to potential indirect effects. Therefore, we designed a system to specifically regulate polySUMOylation of a target protein. GFP binding protein (GBP) is a nanobody fragment with high GFP affinity,[65,66] which allows us to tether SUMO pathway enzymes to a GFP-tagged protein. Because fusing SUMO-conjugating enzyme Ubc9 to a protein increases substrate SUMOylation,[67] we constructed a P_{DDI2}*HA-GBP-UBC9* plasmid (Figure S7A). In this plasmid, hemagglutinin (HA)-GBP-Ubc9 expression is under the control of a *DDI2* promoter, which is induced by cyanamide.[68] Of the two SUMO proteases in budding yeast, Ulp1 exhibits broad activity.[11,12] Thus, we fused the protease domain (PD) of Ulp1 to GBP and generated a P_{DDI2}*HA-GBP-ULP1*^{PD}*-RFP* plasmid (Figures S7B and S7C). Using endogenous Stu2 as a control, the expression of GBP-Ubc9 and GBP-Ulp1^{PD}-RFP was induced efficiently by cyanamide (Figure S7D).

We first tested if expressing HA-GBP-Ubc9 induces polySUMOylation of Tof2-GFP by immunoprecipitating HF-Smt3 from cells growing with cyanamide (Figure S7E). HA-GBP-Ubc9 expression led to smeared Tof2-GFP bands in the IPed samples, indicating Tof2 polySUMOylation. Since Tof2, Net1, and Fob1 are all SUMO substrates and form a complex,[3] recruiting Ubc9 to one protein may lead to SUMOylation of others in the complex. To verify this, we induced HA-GBP-Ubc9 expression in *FOB1-GFP TOF2-13myc*

cells and observed increased SUMOylation of both Fob1-GFP and Tof2-13myc (Figure S7F). However, tethering Ubc9 to the nucleolus did not enhance SUMOylation of the cohesin protein Scc1, a non-nucleolar SUMO substrate (Figure S7G).[69] This result suggests the specificity of GBP-mediated SUMO machinery for proteins within the same complex, which is consistent with the idea of group modification seen in DNA damage response.[70]

PolySUMOylation of Tof2 triggers its delocalization and degradation

Using the GBP tethering system, we investigated how expressing GBP-Ubc9 affects Tof2-GFP localization and turnover. Cells with *P_{DDI2}HA-GBP-UBC9* plasmid were HU arrested, and then GBP-Ubc9 expression was induced by cyanamide. Tof2-GFP intensity and protein level decreased significantly after GBP-Ubc9 induction (Figures 7A, S8A, and S8B). However, this effect was not seen in cells lacking the plasmid. Furthermore, the decrease in Tof2-GFP intensity and protein levels caused by GBP-Ubc9 expression was abolished in *smt3-KRall* and *slx5Δ* mutants (Figures 7A and S8A). Similar trends were observed in nocodazole-arrested cells (Figure S8C). In contrast, targeting Ubc9 to Net1 and Fob1 did not affect their GFP intensity, indicating distinct regulation of Tof2 and Net1/Fob1 (Figure S9). Overall, these findings support the conclusion that targeting the SUMO enzyme Ubc9 to Tof2-GFP results in its nucleolar delocalization and turnover, dependent on polySUMOylation and STUbL activity.

With the *P_{DDI2}HA-GBP-ULP1^{PD}-RFP* plasmid, we assessed if tethering GBP-Ulp1^{PD}-RFP to Tof2-GFP prevents its polySUMOylation induced by Ulp2 nuclear depletion. *ulp2-AA HF-SMT3 TOF2-GFP* cells containing the *P_{DDI2}HA-GBP-ULP1^{PD}-RFP* plasmid were first arrested in S phase with HU. Then rapamycin and the proteasome inhibitor MG132 were added to induce Ulp2 depletion and block Tof2 degradation, respectively. Cell extracts were prepared before and after cyanamide addition to analyze Tof2-GFP SUMOylation. Following IP of Tof2-GFP with an anti-GFP antibody, the accumulation of SUMOylated Tof2-GFP was detected using both anti-FLAG and anti-Smt3 antibodies (Figure S10A). Strikingly, SUMOylated Tof2-GFP species were largely diminished after GBP-Ulp1^{PD}-RFP expression, indicating that GBP-Ulp1^{PD}-RFP indeed abolishes Tof2-GFP SUMOylation. Tethering GBP-Ulp1^{PD} to Fob1-GFP suppresses the SUMOylation of both Fob1-GFP and Tof2-13myc (data not shown), further supporting the idea of group modification.

We next analyzed how GBP-Ulp1^{PD}-RFP expression impacts polySUMO-induced Tof2-GFP delocalization and degradation. Using *ulp2-AA TOF2-GFP* cells with and without *P_{DDI2}HA-GBP-ULP1^{PD}-RFP* plasmid, we first pre-treated HU-arrested cells with cyanamide to induce GBP-Ulp1^{PD}-RFP expression before rapamycin was added to trigger polySUMOylation. In cells lacking *P_{DDI2}HA-GBP-ULP1^{PD}-RFP* plasmid, Tof2-GFP signal declined rapidly after rapamycin treatment (Figure 7B). In *ulp2-AA TOF2-GFP* cells with GBP-Ulp1^{PD}-RFP expression, GBP-Ulp1^{PD}-RFP colocalized with Tof2-GFP, indicating successful tethering. Strikingly, GBP-Ulp1^{PD}-RFP expression led to persistent Tof2-GFP signal after polySUMO induction. A persistent Tof2-GFP protein level was also observed in these cells (Figure S10B), indicating that GBP-Ulp1^{PD}-RFP expression results in a competitive block of polySUMO-induced Tof2-GFP nucleolar delocalization and degradation.

We further utilized Sli15 phosphorylation as a readout to directly assess how Tof2 SUMOylation affects Cdc14 activity. Sli15 is a subunit of the chromosomal passenger complex, and its phosphorylation by CDK is reversed by Cdc14 after FEAR activation.[32] We examined Sli15 dephosphorylation kinetics in *cdc15-2* mutants, wherein the MEN is inactive when grown at 36°C. In Figure S11A, the majority of Sli15 becomes dephosphorylated in *cdc15-2* cells after G_1 release at 36°C for 100 min, as evidenced by increased intensity of the Sli15 bottom band. However, blocking Tof2-GFP polySUMOylation by expressing GBP-Ulp1^{PD} caused less efficient Sli15 dephosphorylation, suggesting that Tof2 polySUMOylation promotes Cdc14 activation.

A SUMO-deficient *tof2* mutant exhibits resistance to polySUMO-induced nucleolar delocalization

To directly assess the role of Tof2 SUMOylation in regulating its nucleolar localization and stability, we sought to abolish Tof2 SUMOylation specifically by generating a SUMO-deficient *tof2* mutant. Across two publications,[59,71] Tof2 has 21 potential SUMOylation sites. The Joined Advanced SUMOylation Site and Sim Analyser (JASSA) predicts 16 SUMOylation sites. To preserve Tof2 functionality, we chose six SUMOylation sites based on overlaps between the publications and JASSA (Figure S11B) and mutated them to arginine, generating a *tof2^{6KR}* plasmid. We then transformed plasmids harboring either *TOF2-GFP-FLAG* or *tof2^{6KR}-GFP-FLAG* into *ulp2-AA* strains to examine Tof2 SUMOylation efficiency. PolySUMOylation was induced in *ulp2-AA* cells with either *TOF2-GFP* or *tof2^{6KR}-GFP*, and Tof2-GFP was IPed with anti-GFP antibody (Figure S11C). Compared to Tof2-GFP, a notable SUMOylation reduction was observed with Tof2^{6KR}-GFP, suggesting that the *tof2^{6KR}* mutant indeed impairs Tof2 SUMOylation.

We next examined delocalization and degradation of SUMO-deficient Tof2 after polySUMOylation induction. As expected, in HU-arrested cells, WT Tof2-GFP underwent significant GFP intensity loss and protein degradation upon triggering polySUMOylation in *ulp2-AA* cells. In contrast, the Tof2-GFP intensity loss and protein turnover were markedly blocked in *tof2^{6KR}* mutants (Figure 7C), confirming the role of Tof2 polySUMOylation in its nucleolar delocalization and degradation. Altogether, our results support the conclusion that polySUMOylation of Tof2 triggers its nucleolar delocalization and degradation, which subsequently promotes Cdc14 nucleolar release for mitotic exit, and this process depends on STUbL and Cdc48 segregase (Figure 7D).

DISCUSSION

We studied how polySUMOylation regulates the Tof2-Net1-Fob1 nucleolar anchor complex for Cdc14 phosphatase in budding yeast. We found that polySUMOylation was cell cycle regulated and crucial for cell cycle progression. Interestingly, Tof2, but not Net1 and Fob1, exhibited cell-cycle-regulated nucleolar turnover. Using chemical-genetic systems, we manipulated protein SUMOylation, and our results revealed that Tof2 polySUMOylation drove its rDNA dissociation and degradation via the polySUMO-STUbL-Cdc48 axis. FEAR, a mitotic exit pathway, likely contributes to nucleolar release of Tof2. Thus, we uncovered a polySUMOylation pathway governing mitotic exit.

In this study, we created chemical-genetic tools to manipulate Tof2 protein SUMOylation. We used the “anchor away” system for nuclear depletion of SUMO protease Ulp2, which induces protein polySUMOylation and leads to Tof2 polySUMOylation, nucleolar delocalization, and degradation. This process relied on polySUMO-induced ubiquitination by STUbL and extraction by Cdc48 segregase. Importantly, Tof2 delocalization and degradation contribute to Cdc14 release and activation for mitotic exit. The results of tethering SUMO machinery to Tof2-GFP, together with the results from SUMO-deficient *tof2* mutants, affirmed that Tof2 polySUMOylation is necessary and sufficient for its nucleolar delocalization and degradation. Overall, these chemical-genetic tools offer valuable insights into SUMO research.

Cdc14 is sequestered within the nucleolus via two anchors, Net1 and Tof2, and the activation of FEAR and MEN enables Cdc14 release.[31] Although Net1 phosphorylation by CDK has been shown to trigger Cdc14 release,[34] the mechanism governing Cdc14 release from Tof2 remains elusive. Here, we uncovered a polySUMO-dependent mechanism for Tof2 delocalization and turnover, which results in Cdc14 release. Interestingly, our results showed that Tof2 turnover is efficient in the MEN mutant *cdc15-2* but is blocked by FEAR mutants. Thus, FEAR likely promotes Tof2 polySUMOylation and the subsequent Cdc14 release.

This study demonstrates the role of the polySUMO axis in protein relocation, which is supported by previous studies. In yeast cells, polySUMOylation recruits STUbL Slx5/Slx8 to persistent DNA break sites, which enables their relocation to the nuclear envelope.[22] Additionally, Mms4, a subunit of Mms4-Mus81 endonuclease, shows proteasomal degradation in a STUbL-dependent manner.[72] The nucleolar release of rDNA repeats during damage repair also depends on SUMOylation and Cdc48 segregase.[64] In human cells, the polySUMO axis is essential for the removal of the chromatin-trapped histone-modifying enzyme PARP1.[73] These studies support the overarching concept that polySUMOylation promotes protein displacement from chromatin.[14] Our work shows polySUMO-dependent Tof2 relocation in the context of the cell cycle. Because many proteins are likely subjected to cell cycle-regulated polySUMOylation, this work opens an avenue to understand how cell cycle regulators are relocalized via polySUMOylation.

Compared to dozens of E3 ubiquitin ligases,[74] only four E3 SUMO ligases have been identified in budding yeast, suggesting that SUMOylation may occur with less specificity than ubiquitination. Indeed, DNA damage triggers simultaneous multisite SUMOylation of several repair proteins, supporting the concept of group modification.[70] The observation of multiple SUMO substrates within a protein complex, including the replisome, the cohesin complex, and KT proteins, also supports this concept.[38,70,75,76] Consistently, we demonstrate SUMOylation of neighboring proteins when SUMO enzymes are recruited to one nucleolar protein. Because of the nature of group modification, SUMOylation may maximize its effect by modifying multiple proteins in a complex.

In summary, the results from this study reveal a polySUMO-dependent mechanism that triggers Tof2 nucleolar delocalization and degradation, ultimately facilitating Cdc14 release for mitotic exit (Figure 7D). We anticipate that polySUMOylation is likely critical to control the subcellular localization of more cell-cycle regulators and other proteins. Because many

cell-cycle regulators are SUMO substrates, such as cohesin, condensin, KT components, and proteins involved in DNA metabolism, it is important to understand how polySUMOylation controls their subcellular localization during the cell cycle.

Limitations of the study

This study reveals that polySUMOylation of the Cdc14 anchor protein Tof2 prompts its delocalization and degradation, which is crucial for Cdc14 release and mitotic progression. A key open question is why Tof2, but not Net1 and Fob1, experiences polySUMO-dependent nucleolar changes. One possibility is that Net1 and Fob1 evade proteasomal degradation after polySUMOylation. Moreover, mass spectrometry identified 21 SUMO-modified lysine residues in Tof2 versus two in Net1,[59,71] raising the possibility that Tof2 is easily recognized by SUMO machinery and the downstream enzymes STUbL and Cdc48.

Interestingly, we found that Tof2 delocalization and degradation depend on FEAR activation rather than MEN, suggesting that FEAR may promote Cdc14 release via Tof2 polySUMOylation. However, how FEAR regulates Tof2 polySUMOylation remains unclear. Notably, Ulp2 nuclear depletion triggered a more robust Cdc14 release than *tof2*Δ mutants in *cdc13-1* arrested cells (Figures S2C and S5A), hinting at an additional mechanism involving Cdc14 SUMOylation. Overall, more work is needed to understand the connection between polySUMOylation and mitotic exit.

While many cell cycle regulators may undergo polySUMO-dependent delocalization and degradation like Tof2, the viability of monoSUMO mutant *smt3-KRall* and STUbL mutants *slx5/8Δ* suggests their non-essential role in cell cycle progression. The polySUMO axis likely aids in many cell-cycle processes, as seen in the slower growth of *smt3-KRall* and *slx5Δ* mutants. We propose that polySUMOylation facilitates macromolecular complex disassembly, possibly alongside redundant pathways, such as other types of modifiction or proteasomal degradation.

In this work, we observed cell-cycle-regulated protein polySUMOylation. However, it remains unclear how polySUMOylation is regulated during the cell cycle. Our previous data show that Polo-like kinase Cdc5 phosphorylates the SUMO protease Ulp2, which likely inactivates Ulp2 to trigger polySUMOylation.[77] Another possibility is that the interaction of SUMO machinery with targeted substrates is regulated, which ensures timely polySUMOylation during the cell cycle, but more research is needed to solidify this idea.

STAR★METHODS

RESOURCES AVAILABILITY

Lead contact—Further information and requests for resources and reagents should be directed to and will be fulfilled by the lead contact, Yanchang Wang (yanchang.wang@med.fsu.edu).

Materials availability—All yeast strains and plasmids generated by this work will be available upon request.

Data and code availability

- Raw data of all experiments have been deposited on Mendeley and are publicly available as of the date of publication. DOI is listed in the key resources table.
- This paper does not report original code.
- Any additional information required to reanalyze the data reported in this paper is available from the lead contact upon request.

EXPERIMENTAL MODEL AND STUDY PARTICIPANT DETAILS

The relevant genotypes and sources of the yeast strains used in this study are listed in Table S1. All the strains listed are isogenic to Y300, a W303 derivative, and they were constructed by tetrad dissection.

Standard protocols for transformation, mating, sporulation, and tetrad dissection were used for yeast strain construction. Unless otherwise noted, cells were grown at 30°C in YPD medium or synthetic dropout medium to maintain selection for plasmids. A PCR-based strategy was used for protein tagging.[78] For cell cycle synchronization, logarithmic cells grown at 30°C were arrested in G_1 phase using 5 μg/mL α-factor for 2–3 h. α-factor was added back after 40-min release to block the following cell cycle. For induction of polySUMOylation, *ulp2-AA* cells were arrested in either HU (Ambeed, Arlington Heights, IL) or nocodazole (Sigma, Burlington, MA) before rapamycin (Thermo, Waltham, MA) was added to a final concentration of 2 μg/mL. For HU arrest, cells in mid-log phase were incubated with 200 μM HU for 2 h. For nocodazole arrest, cells in mid-log phase were treated with 20 μg/mL nocodazole in media containing 1% DMSO for 2 h. Expression of GBP fusion proteins under the *DDI2* promoter was induced by adding cyanamide to a final concentration of 8 mM for 1 h. Yeast growth assays were performed by spotting 10-fold serial dilutions of the indicated strains on solid agar plates.

METHOD DETAILS

Plasmid construction—The plasmids used in this study are listed in Table S2. A PCR-based method was used to construct the *ULP2-FRB-GFP* using template *pFA6a-FRB-GFP-HIS3MX6*.[78] pEGM4 and pEGM5 plasmids were derived from integrating plasmid pRS405.[79] Briefly, P_{DDI2}*HA-GBP-ULP1*^{PD}*-RFP* fragment was synthesized (GenScript, Piscataway, NJ) and then cloned into pRS405. pEGM5 plasmid was generated by amplifying *UBC9* from *S. cerevisiae* genomic DNA before subcloning into pEGM4, replacing *ULP1*^{PD}*-RFP*. For pEGM14 and pEGM15 plasmid constructions, Tof2 was amplified using yeast genomic DNA as a template and cloned into pRS405. For the *tof2*^{6KR} mutant, Gibson assembly method was used for mutagenesis (Molecular Cloning Facility, Florida State University, Tallahassee, FL). All plasmids were verified via DNA sequencing (Sequencing Facility, Florida State University, Tallahassee, FL). Plasmid integration into yeast cells was confirmed by immunoblotting with anti-HA antibody after induction from *DDI2* promoter by adding cyanamide.[68] Primers, sequences, and plasmid maps are available upon request.

Budding index—Cells were taken from culture and fixed with formaldehyde to a final concentration of 3.7%. After sonication, cells were counted and categorized as single cell,

small-budded, and large-budded cells based on the existence and size of the daughter cell. A cell was counted as large budded when the diameter of the daughter cell was greater than half of the diameter of the mother cell. The percentage of large-budded cells (100 cells per time point) was plotted.

Cytological techniques and live-cell imaging—For fluorescence microscopy, collected yeast cells were resuspended in 1 × 3 PBS (pH 7.2) for the examination of fluorescence signals using a microscope with a 60× objective (BZ-X800 from Keyence). For live-cell imaging, glass depression slides were used to prepare an agarose pad filled with complete medium. All live-cell images were acquired at 25°C with a 60× objective lens. A z stack with 11–15 planes of 0.2 μm was acquired for each field and converted to a maximum projection using Keyence BZ-X800 software.

Western blotting—Unless otherwise noted, protein samples were prepared using an alkaline method. Cell pellet from 1 mL of cell culture is resuspended in 200 μL 0.1M NaOH. After 5 min at room temperature, the pellet is collected by centrifugation and resuspended in SDS protein loading buffer. The protein samples were boiled for 5 min and resolved by 10% SDS–PAGE. The resources of the antibodies used in this study are listed in the Key resources table. After ECL (PerkinElmer), western blot membranes were imaged using Bio-Rad ChemiDoc. For visualization of histone H3, membranes were incubated with the secondary antibody for 1 h in the dark. Signals were detected using fluorescently-labeled secondary antibodies on a Li-COR Odyssey CLx imager.

Co-immunoprecipitation (Co-IP)—Cells with HF-Smt3 were grown in 50 mL YPD at 30°C to OD_{600} = 0.75. For the treatment with proteasome inhibitor MG132 (Millipore, MA), cells were first incubated with 0.1% L-Proline and 0.003% SDS for 3 h.[80] Then, MG132 (50 μM) was added for 30 min before harvesting. Harvested cells were resuspended in 700 μL RIPA buffer (50 mM Tris-HCl pH 7.5, 150 mM NaCl, 5 mM EDTA, 0.05% TWEEN 20) supplemented with protease inhibitor cocktail and 20 mM N-ethylmaleimide. Glass beads were added, and cells were lysed by bead bashing. The samples were centrifuged at 15,000 rpm for 10 min at 4°C and the supernatants were kept as cell extracts. Input sample was collected, and the remaining cell extracts were incubated with anti-FLAG beads (Sigma-Aldrich, St. Louis, MO) for 2 h at 4°C. For IP of GFP-tagged proteins, cell lysates were incubated with anti-GFP antibody for 2 h at 4°C. Protein A/G beads were then added, and the lysates were incubated for an additional 2 h. After incubation, the beads were collected by centrifugation and washed three times with RIPA buffer supplied with protease inhibitors. After removal of RIPA buffer, SDS protein loading buffer was added, and the protein samples were incubated for 10 min at 65°C for immunoblotting.

Chromatin fractionation—The chromatin fractionation assay was performed as described in previous works, with minor modifications.[60,61] Briefly, cells were grown in 5 mL YPD at 30°C to OD_{600} = 0.75. Cells were resuspended in extraction buffer (100 mM KCl, 50 mM HEPES-KOH (pH 7.5), 2.5 mM $MgCl_2$, 1% Triton X-100) supplemented with 1 mM DTT, protease inhibitor cocktail, and 20 mM N-ethylmaleimide. Glass beads were added, and cells were lysed by bead bashing. Cell lysates were briefly centrifuged to remove

cell debris. The whole cell extract was applied on top of cushion composed of extraction buffer with 30% sucrose of equal volume. Samples were centrifuged for 20 min at 20,000 g at 4°C. The supernatant containing the soluble protein fraction was carefully collected from the top of the cushion, sucrose was aspirated, and the pellet containing the chromatin fraction was resuspended in sample buffer (8 M urea, 5% SDS, 1 mM EDTA (pH 8.0), 1.5% DTT, 1% bromophenol blue) for subsequent SDS–PAGE and western blotting.

Chromatin immunoprecipitation (ChIP)—ChIP experiments were performed as described previously,[26,58] with some modifications. Briefly, 50 mL cell cultures were grown to OD_{600} = 0.8–1.0, cross-linked with 1% formaldehyde (15 min at room temperature), and then quenched with 200 mM glycine for 10 min. The cells were resuspended in 800 μL of ice-cold lysis buffer with protease inhibitor (0.1% deoxycholic acid, 1 mM EDTA, 50 mM HEPES-KOH (pH 7.5), 140 mM NaCl, 1% Triton X-100). Cells were lysed via bead beating. The chromatin fraction was isolated and sheared to 200–500 bp fragments by sonication (3.5 min, 20 s on/off cycles, 20% amplitude). Lysates were pre-cleared in blocked protein A/G beads for 1 h at 4°C and 50 μL of pre-cleared sample was used as input DNA. Samples were incubated overnight with primary antibody (anti-Myc) at 4°C with constant rotation. Blocked protein A/G beads were added, and samples were further incubated for 2 h. Beads were washed three times with lysis buffer and once with TE (10 mM Tris-HCl pH 8.0, 1 mM EDTA pH 8.0) at room temperature. Beads were eluted by incubating with 100 μL of 50 mM Tris-HCl (pH 8.0), 10 mM EDTA (pH 8.0), and 1% SDS at 65°C for 15 min. The eluates were transferred to fresh tubes and pooled with a final bead wash of 150 μL of TE with 0.67% SDS. To the 50 μL input DNA sample, 200 μL of TE with 1% SDS was added. All samples were incubated at 65°C with proteinase K to reverse crosslinking. DNA was cleaned up with E-Z 96 Cycle Pure Kit and eluted with 50 μL of water. The IPed samples were diluted 1:8 in molecular grade water. The inputs were diluted 1:2000 in water. Primer pairs (primer pair “15” for rDNA; *CUP1* for negative control) were used as described.[26] Individual PCR reactions were 10 μL and consisted of 5 μL AccuStart II PCR SuperMix (Quantabio, Beverly, MA), 1 μL diluted DNA, and 4 μL 2 μM primer pair. PCR parameters were one cycle of 95°C for 2 min, 55°C for 30 s, and 72°C for 1 min, followed by 21 cycles of 95°C for 30 s, 55°C for 30 s, and 72°C for 1 min, and a final step of 72°C for 4 min. The relative fold enrichment was calculated by averaging triplicates of each reaction and calculating the ratio of rDNA to *CUP1* enrichment in the IPed samples and comparing this with the rDNA/*CUP1* ratio in the input samples. This is represented in the following calculation:

$$\frac{[\text{rDNA(IP)/CUP1(IP)}]}{[\text{rDNA(Input)/CUP1(Input)}]}$$

Fluorescence intensity analysis—Fluorescence intensity analysis was determined by measuring the signal intensity using ImageJ. A region of interest (ROI) harboring the fluorescence signal was selected for each cell using the Wand tool, which traces regions of uniform color that form a contiguous area. Tolerance threshold for uniform color was optimized for each set of experiments for precise ROI delineation. The average intensity per pixel for that region was multiplied by the total area to determine total fluorescence

intensity. The ROI was moved to a region in the cell with no observable fluorescence to calculate the total background intensity, and this value was used to normalize the signal intensity. At least 50 cells were counted for each strain and timepoint. The signal intensity levels are represented as mean ± SD and were plotted using Graph Pad/Prism software.

$$Total\ fluorescence\ intensity_{normalized} = (Mean\ intensity_{ROI} \times Area_{ROI}) - (Mean\ intensity_{background} \times Area_{background})$$

QUANTIFICATION AND STATISTICAL ANALYSIS

All statistical analyses and graph preparations were done using Graph Pad/Prism software. Unless indicated otherwise, results from fluorescence microscopy experiments were determined by counting at least 50 cells for each yeast strain. Experiments repeated twice or three times are indicated as such. The mean values were calculated and shown with corresponding standard deviations in bar graphs. We performed unpaired *t*-tests, one-way ANOVAs, or two-way ANOVAs and the significance was corrected for multiple comparisons using Tukey's correction to generate a significance of $*p < 0.05$, $**p < 0.01$, $***p < 0.001$, or $****p < 0.0001$ and is denoted as such. To determine Cdc14-GFP nucleolar localization, a ROI harboring the Cdc14-GFP signal was selected for each cell using the Wand tool in ImageJ. This ROI was used to measure both Nop1-mApple (nucleolar marker) and Cdc14-GFP mean signal intensities, and all graphs are plotted as ratios (Nop1-mApple/Cdc14-GFP). To determine differences in Tof2 protein levels, we used ImageJ to acquire the intensity of each protein band from western blotting images. Then, the protein levels were normalized by determining the ratio to loading control, Pgk1.

Supplementary Material

Refer to Web version on PubMed Central for supplementary material.

ACKNOWLEDGMENTS

We are grateful to the yeast community at Florida State University for reagents and helpful suggestions. The *smt3-KRall (*HY8053) strain was a kind gift from Dr. Dana Branzei at the FIRC Institute of Molecular Oncology in Milan, Italy. The $ufd1^{\Delta SIM}$ strain (MCO160) was a kind gift from Dr. Sigurd Braun at the Ludwig Maximilian University in Munich, Germany. We thank Dr. Danesh Moazed at Harvard University (Boston, MA, USA) for *RDN1:ADE2* strains. We received the H3 antibody from Dr. Akash Gunjan (Florida State University). We thank Cheryl Pye from the Biology Core Facility at Florida State University for help with $tof2^{6kr}$ plasmid construction. We thank Dr. Sue Biggins at Fred Hutchinson Cancer Research Center for providing the *FIN1-GFP* (pSB1252) plasmid. The *mms21-11-LEU2* strain was a kind gift from Dr. Xiaolan Zhao from Sloan Kettering Institute. We thank Drs. Timothy Megraw, Richard Nowakowski, and Terra Bradley for critical reading of this manuscript. This work was supported by R01GM151447 from the NIH (to Y.W.).

REFERENCES

1. Geiss-Friedlander R, and Melchior F (2007). Concepts in sumoylation: a decade on. Nat. Rev. Mol. Cell Biol 8, 947–956. 10.1038/nrm2293. [PubMed: 18000527]
2. Wohlschlegel JA, Johnson ES, Reed SI, and Yates JR (2004). Global analysis of protein sumoylation in Saccharomyces cerevisiae. J. Biol. Chem 279, 45662–45668. 10.1074/jbc.M409203200. [PubMed: 15326169]

3. Albuquerque CP, Wang G, Lee NS, Kolodner RD, Putnam CD, and Zhou H (2013). Distinct SUMO Ligases Cooperate with Esc2 and Slx5 to Suppress Duplication-Mediated Genome Rearrangements. PLoS Genet. 9, e1003670. 10.1371/journal.pgen.1003670. [PubMed: 23935535]
4. Guerra de Souza AC, Prediger RD, and Cimarosti H (2016). SUMO-regulated mitochondrial function in Parkinson's disease. J. Neurochem 137, 673–686. 10.1111/jnc.13599. [PubMed: 26932327]
5. Han ZJ, Feng YH, Gu BH, Li YM, and Chen H (2018). The post-translational modification, SUMOylation, and cancer (Review). Int. J. On-col 52, 1081–1094. 10.3892/ijo.2018.4280.
6. Kerscher O, Felberbaum R, and Hochstrasser M (2006). Modification of proteins by ubiquitin and ubiquitin-like proteins. Annu. Rev. Cell Dev. Biol 22, 159–180. 10.1146/annurev.cellbio.22.010605.093503. [PubMed: 16753028]
7. Capili AD, and Lima CD (2007). Structure and analysis of a complex between SUMO and Ubc9 illustrates features of a conserved E2-Ubl interaction. J. Mol. Biol 369, 608–618. 10.1016/j.jmb.2007.04.006. [PubMed: 17466333]
8. Zhao X, and Blobel G (2005). A SUMO ligase is part of a nuclear multi-protein complex that affects DNA repair and chromosomal organization. Proc. Natl. Acad. Sci. USA 102, 4777–4782. 10.1073/pnas.0500537102. [PubMed: 15738391]
9. Johnson ES, and Gupta AA (2001). An E3-like factor that promotes SUMO conjugation to the yeast septins. Cell 106, 735–744. 10.1016/s0092-8674(01)00491-3. [PubMed: 11572779]
10. Takahashi Y, Kahyo T, Toh-E A, Yasuda H, and Kikuchi Y (2001). Yeast Ull1/Siz1 is a novel SUMO1/Smt3 ligase for septin components and functions as an adaptor between conjugating enzyme and substrates. J. Biol. Chem 276, 48973–48977. 10.1074/jbc.M109295200. [PubMed: 11577116]
11. Mossessova E, and Lima CD (2000). Ulp1-SUMO crystal structure and genetic analysis reveal conserved interactions and a regulatory element essential for cell growth in yeast. Mol. Cell 5, 865–876. 10.1016/s1097-2765(00)80326-3. [PubMed: 10882122]
12. Li SJ, and Hochstrasser M (2003). The Ulp1 SUMO isopeptidase: distinct domains required for viability, nuclear envelope localization, and substrate specificity. J. Cell Biol 160, 1069–1081. 10.1083/jcb.200212052. [PubMed: 12654900]
13. Kramarz K, Schirmeisen K, Boucherit V, Ait Saada A, Lovo C, Palancade B, Freudenreich C, and Lambert SAE (2020). The nuclear pore primes recombination-dependent DNA synthesis at arrested forks by promoting SUMO removal. Nat. Commun 11, 5643. 10.1038/s41467-020-19516-z. [PubMed: 33159083]
14. Keiten-Schmitz J, Schunck K, and Müller S (2019). SUMO Chains Rule on Chromatin Occupancy. Front. Cell Dev. Biol 7, 343. 10.3389/fcell.2019.00343. [PubMed: 31998715]
15. Banani SF, Rice AM, Peeples WB, Lin Y, Jain S, Parker R, and Rosen MK (2016). Compositional Control of Phase-Separated Cellular Bodies. Cell 166, 651–663. 10.1016/j.cell.2016.06.010. [PubMed: 27374333]
16. Min J, Wright WE, and Shay JW (2019). Clustered telomeres in phase-separated nuclear condensates engage mitotic DNA synthesis through BLM and RAD52. Genes Dev. 33, 814–827. 10.1101/gad.324905.119. [PubMed: 31171703]
17. Xie Y, Kerscher O, Kroetz MB, McConchie HF, Sung P, and Hochstrasser M (2007). The yeast Hex3.Slx8 heterodimer is a ubiquitin ligase stimulated by substrate sumoylation. J. Biol. Chem 282, 34176–34184. 10.1074/jbc.M706025200. [PubMed: 17848550]
18. Mullen JR, and Brill SJ (2008). Activation of the Slx5-Slx8 ubiquitin ligase by poly-small ubiquitin-like modifier conjugates. J. Biol. Chem 283, 19912–19921. 10.1074/jbc.M802690200. [PubMed: 18499666]
19. Prudden J, Pebernard S, Raffa G, Slavin DA, Perry JJP, Tainer JA, McGowan CH, and Boddy MN (2007). SUMO-targeted ubiquitin ligases in genome stability. EMBO J. 26, 4089–4101. 10.1038/sj.emboj.7601838. [PubMed: 17762865]
20. Bergink S, Ammon T, Kern M, Schermelleh L, Leonhardt H, and Jentsch S (2013). Role of Cdc48/p97 as a SUMO-targeted segregase curbing Rad51-Rad52 interaction. Nat. Cell Biol 15, 526–532. 10.1038/ncb2729. [PubMed: 23624404]

21. Folger A, and Wang Y (2021). The Cytotoxicity and Clearance of Mutant Huntingtin and Other Misfolded Proteins. Cells 10, 2835. [PubMed: 34831058]
22. Horigome C, Bustard DE, Marcomini I, Delgoshaie N, Tsai-Pflug-felder M, Cobb JA, and Gasser SM (2016). PolySUMOylation by Siz2 and Mms21 triggers relocation of DNA breaks to nuclear pores through the Slx5/Slx8 STUbL. Genes Dev. 30, 931–945. 10.1101/gad.277665.116. [PubMed: 27056668]
23. Whalen JM, Dhingra N, Wei L, Zhao X, and Freudenreich CH (2020). Relocation of Collapsed Forks to the Nuclear Pore Complex Depends on Sumoylation of DNA Repair Proteins and Permits Rad51 Association. Cell Rep. 31, 107635. 10.1016/j.celrep.2020.107635. [PubMed: 32402281]
24. Srikumar T, Lewicki MC, Costanzo M, Tkach JM, van Bakel H, Tsui K, Johnson ES, Brown GW, Andrews BJ, Boone C, et al. (2013). Global analysis of SUMO chain function reveals multiple roles in chromatin regulation. J. Cell Biol 201, 145–163. 10.1083/jcb.201210019. [PubMed: 23547032]
25. Krawczyk C, Dion V, Schär P, and Fritsch O (2014). Reversible Top1 cleavage complexes are stabilized strand-specifically at the ribosomal replication fork barrier and contribute to ribosomal DNA stability. Nucleic Acids Res. 42, 4985–4995. 10.1093/nar/gku148. [PubMed: 24574527]
26. Huang J, Brito IL, Villén J, Gygi SP, Amon A, and Moazed D (2006). Inhibition of homologous recombination by a cohesin-associated clamp complex recruited to the rDNA recombination enhancer. Genes Dev. 20, 2887–2901. 10.1101/gad.1472706. [PubMed: 17043313]
27. Visintin R, Craig K, Hwang ES, Prinz S, Tyers M, and Amon A (1998). The phosphatase Cdc14 triggers mitotic exit by reversal of Cdk-dependent phosphorylation. Mol. Cell 2, 709–718. [PubMed: 9885559]
28. Visintin R, Hwang ES, and Amon A (1999). Cfi1 prevents premature exit from mitosis by anchoring Cdc14 phosphatase in the nucleolus. Nature 398, 818–823. 10.1038/19775. [PubMed: 10235265]
29. Shou W, Seol JH, Shevchenko A, Baskerville C, Moazed D, Chen ZW, Jang J, Shevchenko A, Charbonneau H, and Deshaies RJ (1999). Exit from mitosis is triggered by Tem1-dependent release of the protein phosphatase Cdc14 from nucleolar RENT complex. Cell 97, 233–244. [PubMed: 10219244]
30. Waples WG, Chahwan C, Ciechonska M, and Lavoie BD (2009). Putting the brake on FEAR: Tof2 promotes the biphasic release of Cdc14 phosphatase during mitotic exit. Mol. Biol. Cell 20, 245–255. 10.1091/mbc.E08-08-0879. [PubMed: 18923139]
31. Stegmeier F, Visintin R, and Amon A (2002). Separase, polo kinase, the kinetochore protein Slk19, and Spo12 function in a network that controls Cdc14 localization during early anaphase. Cell 108, 207–220. 10.1016/s0092-8674(02)00618-9. [PubMed: 11832211]
32. Jin F, Liu H, Liang F, Rizkallah R, Hurt MM, and Wang Y (2008). Temporal control of the dephosphorylation of Cdk substrates by mitotic exit pathways in budding yeast. Proc. Natl. Acad. Sci. USA 105, 16177–16182. 10.1073/pnas.0808719105. [PubMed: 18845678]
33. Liang F, Jin F, Liu H, and Wang Y (2009). The molecular function of the yeast polo-like kinase Cdc5 in Cdc14 release during early anaphase. Mol. Biol. Cell 20, 3671–3679. 10.1091/mbc.e08-10-1049. [PubMed: 19570916]
34. Azzam R, Chen SL, Shou W, Mah AS, Alexandru G, Nasmyth K, Annan RS, Carr SA, and Deshaies RJ (2004). Phosphorylation by cyclin B-Cdk underlies release of mitotic exit activator Cdc14 from the nucleolus. Science 305, 516–519. 10.1126/science.1099402. [PubMed: 15273393]
35. Queralt E, Lehane C, Novak B, and Uhlmann F (2006). Downregulation of PP2A(Cdc55) phosphatase by separase initiates mitotic exit in budding yeast. Cell 125, 719–732. [PubMed: 16713564]
36. Wang Y, and Ng TY (2006). Phosphatase 2A Negatively Regulates Mitotic Exit in Saccharomyces cerevisiae. Mol. Biol. Cell 17, 80–89. [PubMed: 16079183]
37. Psakhye I, Castellucci F, and Branzei D (2019). SUMO-Chain-Regulated Proteasomal Degradation Timing Exemplified in DNA Replication Initiation. Mol. Cell 76, 632–645.e6. 10.1016/j.molcel.2019.08.003. [PubMed: 31519521]

38. Su XB, Wang M, Schaffner C, Nerusheva OO, Clift D, Spanos C, Kelly DA, Tatham M, Wallek A, Wu Y, et al. (2021). SUMOylation stabilizes sister kinetochore biorientation to allow timely anaphase. J. Cell Biol 220, e202005130. 10.1083/jcb.202005130.
39. Ohkuni K, Takahashi Y, and Basrai MA (2015). Protein purification technique that allows detection of sumoylation and ubiquitination of budding yeast kinetochore proteins Ndc10 and Ndc80. J. Vis. Exp 99, e52482. 10.3791/52482.
40. Cohen-Fix O, Peters JM, Kirschner MW, and Koshland D (1996). Anaphase initiation in Saccharomyces cerevisiae is controlled by the APC-dependent degradation of the anaphase inhibitor Pds1p. Genes Dev. 10, 3081–3093. [PubMed: 8985178]
41. Ryu HY, López-Giráldez F, Knight J, Hwang SS, Renner C, Kreft SG, and Hochstrasser M (2018). Distinct adaptive mechanisms drive recovery from aneuploidy caused by loss of the Ulp2 SUMO protease. Nat. Commun 9, 5417. 10.1038/s41467-018-07836-0. [PubMed: 30575729]
42. Bremmer SC, Hall H, Martinez JS, Eissler CL, Hinrichsen TH, Rossie S, Parker LL, Hall MC, and Charbonneau H (2012). Cdc14 phosphatases preferentially dephosphorylate a subset of cyclin-dependent kinase (Cdk) sites containing phosphoserine. J. Biol. Chem 287, 1662–1669. 10.1074/jbc.M111.281105. [PubMed: 22117071]
43. Bokros M, Gravenmier C, Jin F, Richmond D, and Wang Y (2016). Fin1-PP1 Helps Clear Spindle Assembly Checkpoint Protein Bub1 from Kinetochores in Anaphase. Cell Rep. 14, 1074–1085. 10.1016/j.celrep.2016.01.007. [PubMed: 26832405]
44. Liang F, and Wang Y (2007). DNA damage checkpoints inhibit mitotic exit by two different mechanisms. Mol. Cell Biol 27, 5067–5078. 10.1128/mcb.00095-07. [PubMed: 17485442]
45. Bylebyl GR, Belichenko I, and Johnson ES (2003). The SUMO isopeptidase Ulp2 prevents accumulation of SUMO chains in yeast. J. Biol. Chem 278, 44113–44120. 10.1074/jbc.M308357200. [PubMed: 12941945]
46. Geil C, Schwab M, and Seufert W (2008). A nucleolus-localized activator of Cdc14 phosphatase supports rDNA segregation in yeast mitosis. Curr. Biol 18, 1001–1005. 10.1016/j.cub.2008.06.025. [PubMed: 18595708]
47. Li SJ, and Hochstrasser M (2000). The yeast ULP2 (SMT4) gene encodes a novel protease specific for the ubiquitin-like Smt3 protein. Mol. Cell Biol 20, 2367–2377. 10.1128/mcb.20.7.2367-2377.2000. [PubMed: 10713161]
48. D'Amours D, Stegmeier F, and Amon A (2004). Cdc14 and condensin control the dissolution of cohesin-independent chromosome linkages at repeated DNA. Cell 117, 455–469. [PubMed: 15137939]
49. Sullivan M, Higuchi T, Katis VL, and Uhlmann F (2004). Cdc14 phosphatase induces rDNA condensation and resolves cohesin-independent cohesion during budding yeast anaphase. Cell 117, 471–482. [PubMed: 15137940]
50. Lafontaine DLJ, Riback JA, Bascetin R, and Brangwynne CP (2021). The nucleolus as a multiphase liquid condensate. Nat. Rev. Mol. Cell Biol 22, 165–182. 10.1038/s41580-020-0272-6. [PubMed: 32873929]
51. Jacquiau HR, van Waardenburg RCAM, Reid RJD, Woo MH, Guo H, Johnson ES, and Bjornsti MA (2005). Defects in SUMO (small ubiquitin-related modifier) conjugation and deconjugation alter cell sensitivity to DNA topoisomerase I-induced DNA damage. J. Biol. Chem 280, 23566–23575. 10.1074/jbc.M500947200. [PubMed: 15817450]
52. Cheng CH, Lo YH, Liang SS, Ti SC, Lin FM, Yeh CH, Huang HY, and Wang TF (2006). SUMO modifications control assembly of synaptonemal complex and polycomplex in meiosis of Saccharomyces cerevisiae. Genes Dev. 20, 2067–2081. 10.1101/gad.1430406. [PubMed: 16847351]
53. Abraham NM, Ramalingam K, Murthy S, and Mishra K (2019). Siz2 Prevents Ribosomal DNA Recombination by Modulating Levels of Tof2 in Saccharomyces cerevisiae. mSphere 4, e00713–19. 10.1128/mSphere.00713-19. [PubMed: 31776241]
54. Schwienhorst I, Johnson ES, and Dohmen RJ (2000). SUMO conjugation and deconjugation. Mol. Gen. Genet 263, 771–786. 10.1007/s004380000254. [PubMed: 10905345]

55. Bachant J, Alcasabas A, Blat Y, Kleckner N, and Elledge SJ (2002). The SUMO-1 isopeptidase Smt4 is linked to centromeric cohesion through SUMO-1 modification of DNA topoisomerase II. Mol. Cell 9, 1169–1182. [PubMed: 12086615]
56. Haruki H, Nishikawa J, and Laemmli UK (2008). The anchor-away technique: rapid, conditional establishment of yeast mutant phenotypes. Mol. Cell 31, 925–932. 10.1016/j.molcel.2008.07.020. [PubMed: 18922474]
57. Kroetz MB, Su D, and Hochstrasser M (2009). Essential Role of Nuclear Localization for Yeast Ulp2 SUMO Protease Function. Mol. Biol. Cell 20, 2196–2206. 10.1091/mbc.e08-10-1090. [PubMed: 19225149]
58. Gillies J, Hickey CM, Su D, Wu Z, Peng J, and Hochstrasser M (2016). SUMO Pathway Modulation of Regulatory Protein Binding at the Ribosomal DNA Locus in Saccharomyces cerevisiae. Genetics 202, 1377–1394. 10.1534/genetics.116.187252. [PubMed: 26837752]
59. Liang J, Singh N, Carlson CR, Albuquerque CP, Corbett KD, and Zhou H (2017). Recruitment of a SUMO isopeptidase to rDNA stabilizes silencing complexes by opposing SUMO targeted ubiquitin ligase activity. Genes Dev. 31, 802–815. 10.1101/gad.296145.117. [PubMed: 28487408]
60. Liang C, and Stillman B (1997). Persistent initiation of DNA replication and chromatin-bound MCM proteins during the cell cycle in cdc6 mutants. Genes Dev. 11, 3375–3386. 10.1101/gad.11.24.3375. [PubMed: 9407030]
61. Wang AY, Schulze JM, Skordalakes E, Gin JW, Berger JM, Rine J, and Kobor MS (2009). Asf1-like structure of the conserved Yaf9 YEATS domain and role in H2A.Z deposition and acetylation. Proc. Natl. Acad. Sci. USA 106, 21573–21578. 10.1073/pnas.0906539106. [PubMed: 19966225]
62. Ghislain M, Udvardy A, and Mann C (1993). S. cerevisiae 26S protease mutants arrest cell division in G2/metaphase. Nature 366, 358–362. 10.1038/366358a0. [PubMed: 8247132]
63. Nie M, Aslanian A, Prudden J, Heideker J, Vashisht AA, Wohlschlegel JA, Yates JR, and Boddy MN (2012). Dual recruitment of Cdc48 (p97)-Ufd1-Npl4 ubiquitin-selective segregase by small ubiquitin-like modifier protein (SUMO) and ubiquitin in SUMO-targeted ubiquitin ligase-mediated genome stability functions. J. Biol. Chem 287, 29610–29619. 10.1074/jbc.M112.379768. [PubMed: 22730331]
64. Capella M, Mandemaker IK, Martín Caballero L, den Brave F, Pfander B, Ladurner AG, Jentsch S, and Braun S (2021). Nucleolar release of rDNA repeats for repair involves SUMO-mediated untethering by the Cdc48/p97 segregase. Nat. Commun 12, 4918. 10.1038/s41467-021-25205-2. [PubMed: 34389719]
65. Rothbauer U, Zolghadr K, Muyldermans S, Schepers A, Cardoso MC, and Leonhardt H (2008). A versatile nanotrap for biochemical and functional studies with fluorescent fusion proteins. Mol. Cell. Proteomics 7, 282–289. 10.1074/mcp.M700342-MCP200. [PubMed: 17951627]
66. Rothbauer U, Zolghadr K, Tillib S, Nowak D, Schermelleh L, Gahl A, Backmann N, Conrath K, Muyldermans S, Cardoso MC, and Leonhardt H (2006). Targeting and tracing antigens in live cells with fluorescent nanobodies. Nat. Methods 3, 887–889. 10.1038/nmeth953. [PubMed: 17060912]
67. Jakobs A, Koehnke J, Himstedt F, Funk M, Korn B, Gaestel M, and Niedenthal R (2007). Ubc9 fusion-directed SUMOylation (UFDS): a method to analyze function of protein SUMOylation. Nat. Methods 4, 245–250. 10.1038/nmeth1006. [PubMed: 17277783]
68. Lin A, Zeng C, Wang Q, Zhang W, Li M, Hanna M, and Xiao W (2018). Utilization of a Strongly Inducible DDI2 Promoter to Control Gene Expression in Saccharomyces cerevisiae. Front. Microbiol 9, 2736. 10.3389/fmicb.2018.02736. [PubMed: 30505295]
69. Wu N, Kong X, Ji Z, Zeng W, Potts PR, Yokomori K, and Yu H (2012). Scc1 sumoylation by Mms21 promotes sister chromatid recombination through counteracting Wapl. Genes Dev. 26, 1473–1485. 10.1101/gad.193615.112. [PubMed: 22751501]
70. Psakhye I, and Jentsch S (2012). Protein group modification and synergy in the SUMO pathway as exemplified in DNA repair. Cell 151, 807–820. 10.1016/j.cell.2012.10.021. [PubMed: 23122649]
71. Bhagwat NR, Owens SN, Ito M, Boinapalli JV, Poa P, Ditzel A, Kopparapu S, Mahalawat M, Davies OR, Collins SR, et al. (2021). SUMO is a pervasive regulator of meiosis. Elife 10, e57720. 10.7554/eLife.57720. [PubMed: 33502312]

72. Waizenegger A, Urulangodi M, Lehmann CP, Reyes TAC, Saugar I, Tercero JA, Szakal B, and Branzei D (2020). Mus81-Mms4 endonuclease is an Esc2-STUbL-Cullin8 mitotic substrate impacting on genome integrity. Nat. Commun 11, 5746. 10.1038/s41467-020-19503-4. [PubMed: 33184279]

73. Krastev DB, Li S, Sun Y, Wicks AJ, Hoslett G, Weekes D, Badder LM, Knight EG, Marlow R, Pardo MC, et al. (2022). The ubiquitin-dependent ATPase p97 removes cytotoxic trapped PARP1 from chromatin. Nat. Cell Biol 24, 62–73. 10.1038/s41556-021-00807-6. [PubMed: 35013556]

74. Finley D, Ulrich HD, Sommer T, and Kaiser P (2012). The ubiquitin-proteasome system of Saccharomyces cerevisiae. Genetics 192, 319–360. 10.1534/genetics.112.140467. [PubMed: 23028185]

75. Zhou W, Ryan JJ, and Zhou H (2004). Global Analyses of Sumoylated Proteins in Saccharomyces cerevisiae: INDUCTION OF PROTEIN SUMOYLATION BY CELLULAR STRESSES. J. Biol. Chem 279, 32262–32268. [PubMed: 15166219]

76. Wei L, and Zhao X (2017). Roles of SUMO in Replication Initiation, Progression, and Termination. Adv. Exp. Med. Biol 1042, 371–393. 10.1007/978-981-10-6955-0_17. [PubMed: 29357067]

77. Baldwin ML, Julius JA, Tang X, Wang Y, and Bachant J (2009). The yeast SUMO isopeptidase Smt4/Ulp2 and the polo kinase Cdc5 act in an opposing fashion to regulate sumoylation in mitosis and cohesion at centromeres. Cell Cycle 8, 3406–3419. 10.4161/cc.8.20.9911. [PubMed: 19823017]

78. Longtine MS, McKenzie A 3rd, Demarini DJ, Shah NG, Wach A, Brachat A, Philippsen P, and Pringle JR (1998). Additional modules for versatile and economical PCR-based gene deletion and modification in Saccharomyces cerevisiae. Yeast 14, 953–961. [PubMed: 9717241]

79. Sikorski RS, and Hieter P (1989). A system of shuttle vectors and yeast host strains designed for efficient manipulation of DNA in Saccharomyces cerevisiae. Genetics 122, 19–27. [PubMed: 2659436]

80. Chuang KH, Liang F, Higgins R, and Wang Y (2016). Ubiquilin/Dsk2 promotes inclusion body formation and vacuole (lysosome)-mediated disposal of mutated huntingtin. Mol. Biol. Cell 27, 2025–2036. 10.1091/mbc.E16-01-0026. [PubMed: 27170182]

Highlights

- Protein polySUMOylation is a cell-cycle-regulated process in budding yeast
- The localization and abundance of Cdc14 nucleolar anchor Tof2 fluctuate during the cell cycle
- PolySUMO-triggered Tof2 ubiquitination and extraction cause its delocalization and degradation
- PolySUMO-mediated Tof2 delocalization promotes Cdc14 activation and mitotic exit

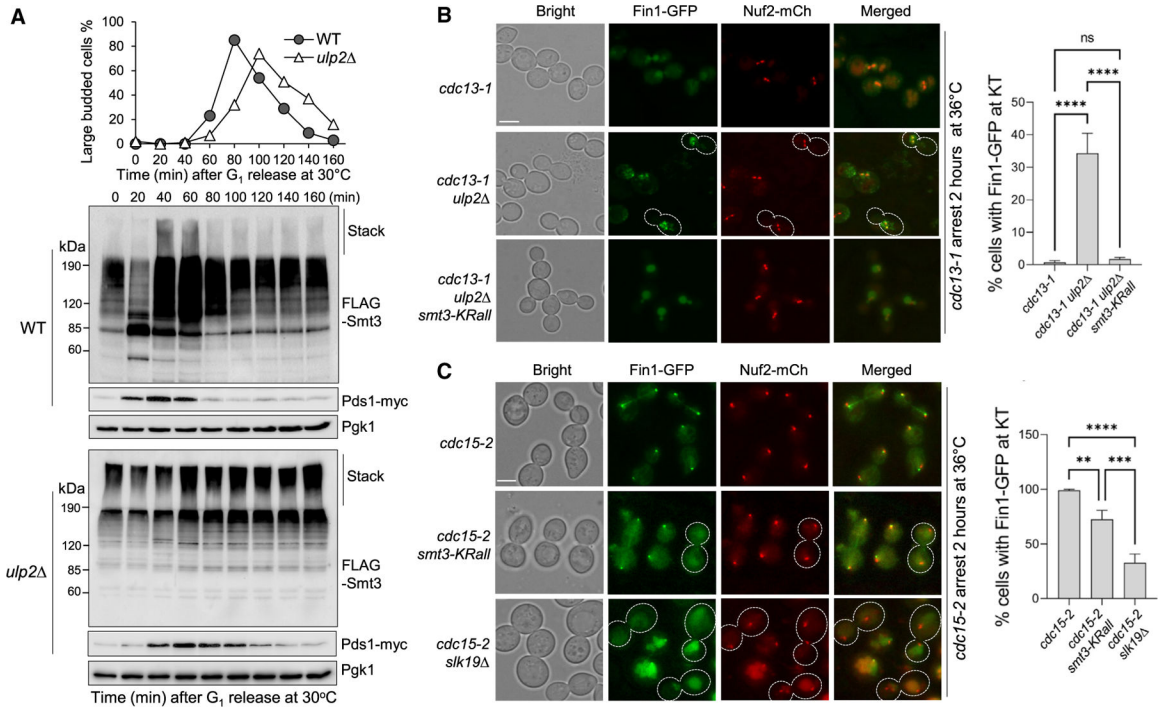

Figure 1. PolySUMOylation is cell cycle regulated and critical for robust mitotic exit

(A) PolySUMOylation during the cell cycle in WT and *ulp2Δ* cells. G_1-arrested WT (4677-3-2) and *ulp2Δ* (4686-5-2) cells with His-FLAG (HF)-Smt3 and Pds1-18myc were released. Cells were collected every 20 min for western blotting and budding index. Pgk1, loading control.

(B) Enhanced polySUMOylation in *ulp2Δ* cells causes premature mitotic exit, as indicated by Fin1-GFP KT localization. Asynchronous *cdc13-1* (4115-2-3), *cdc13-1 ulp2Δ* (4145-3-2), and *cdc13-1 ulp2Δ smt3-KRall* (4689-1-1) cells with *FIN1-GFP* (pSB1252) plasmids were cultured at 25°C and then shifted to 36°C for 2 h for *cdc13-1* arrest. Fin1-GFP KT localization in representative cells is shown on the left. Cells with a white-dotted boundary show Fin1-GFP KT localization. Nuf2-mCherry (Nuf2-mCh) marks KTs. Scale bar, 5 μm. Fin1 KT localization was quantified after three repeats. Statistical analysis used one-way ANOVA with Tukey's test. Bars represent mean values ± SD.

(C) PolySUMO-deficient mutant *smt3-KRall* delays Fin1-GFP KT localization during the cell cycle. Asynchronous *cdc15-2* (4635-2-2), *cdc15-2 smt3-KRall* (4635-3-3), and *cdc15-2 slk19Δ* (4684-5-2) cells with *FIN1-GFP* at 25°C were shifted to 36°C for 2 h for *cdc15-2* arrest. Fin1-GFP KT localization in representative cells is shown on the left. Cells with a white-dotted boundary lack Fin1-GFP KT localization. Scale bar, 5 μm. The statistical analysis is the same as in (B). Bars represent mean values ± SD.

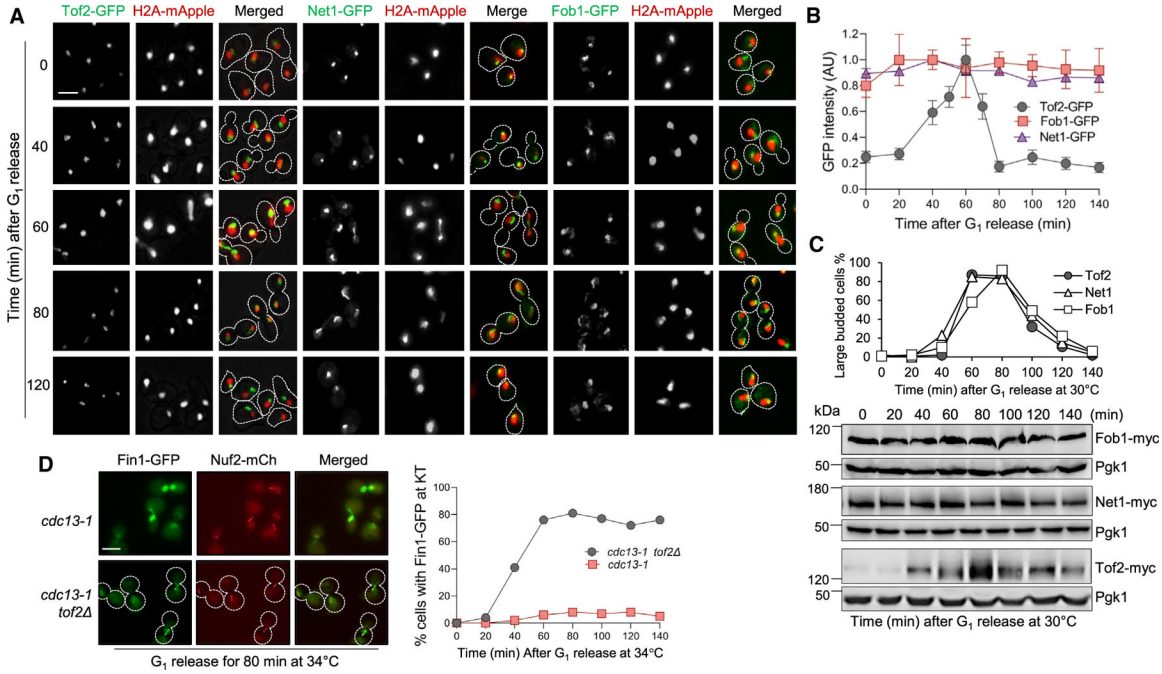

Figure 2. The abundance of the nucleolar protein Tof2, but not Net1 or Fob1, is cell-cycle regulated

(A) The intensity Tof2-GFP, but not Net1/Fob1-GFP, peaks before anaphase onset. Shown are representative images for Tof2-GFP (4329-2-4), Net1-GFP (3727-9-1), and Fob1-GFP (4567-1-3) intensity during the cell cycle. G_1-arrested cells were released into 30°C YPD (yeast extract, peptone, dextrose). H2A-mApple marks nuclear division. Scale bar, 5 μm.

(B) GFP intensity (n = 50 cells) was calculated as described in STAR Methods. The line graph represents mean values ±SD.

(C) The protein levels of Tof2-13myc (YYW273), Net1-9myc (405-4-2), and Fob1-13myc (EGM13) during the cell cycle. G_1-arrested cells were released into 30°C YPD and collected every 20 min for protein levels and budding index. Pgk1, loading control.

(D) Premature mitotic exit in *tof2Δ* mutants. *cdc13-1 NUF2-mCherry* (4115-2-3) and *cdc13-1 NUF2-mCherry tof2Δ* (4126-1-4) cells harboring *FIN1-GFP* at 25°C were arrested in G_1 and then released at 34°C. Fin1-GFP colocalization with Nuf2-mCherry (KT marker) was counted (n = 100) over time. Representative cells 80 min following G_1 release are shown. Cells with a white-dotted boundary show premature Fin1-GFP KT localization. Scale bar, 5 μm.

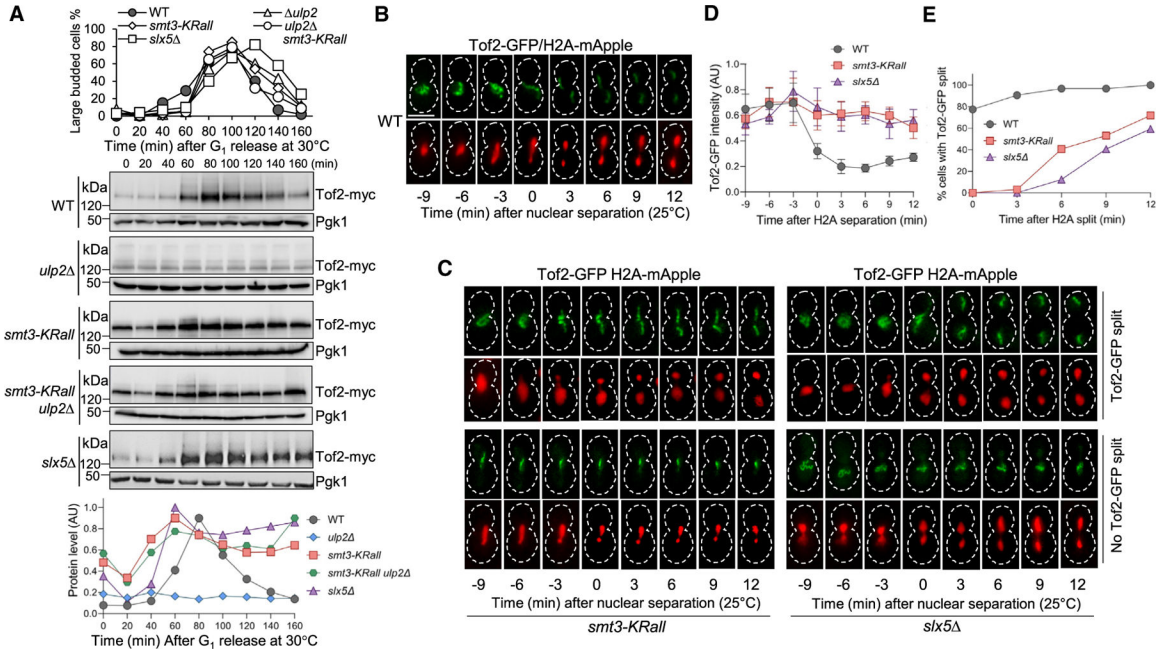

Figure 3. PolySUMOylation regulates Tof2 protein localization and turnover

(A) Tof2 protein level and modification during the cell cycle in SUMO mutants. G_1-arrested WT (YYW273), *ulp2Δ* (4136-1-4), *smt3-KRall* (4386-3-1), *ulp2Δ smt3-KRall* (4396-1-2), and *slx5Δ* (4125-3-4) cells with Tof2-13myc were released and collected every 20 min. Tof2-13myc protein levels were detected by western blotting and normalized to the loading control Pgk1.

(B) Live-cell imaging of Tof2-GFP/H2A-mApple in WT (4329-2-4) cells. Log-phase cells were spotted onto the surface of a slide covered with agarose medium and subjected to live-cell microscopy at 25°C. H2A-mApple separation marks time = 0 min. Scale bar, 5 μm.

(C) *smt3-KRall* and *slx5Δ* mutants show persistent Tof2-GFP intensity and a dramatic delay in Tof2-GFP separation. *smt3-KRall* (4351-1-3) and *slx5Δ* (4356-4-3) cells containing Tof2-GFP were treated the same as in (B).

(D) Tof2-GFP intensity from cells in (B) and (C) was quantified. The line graph represents mean values ± SD.

(E) Percentage of cells (n = 30 Cells) that showed Tof2-GFP separation following nuclear segregation in live cells.

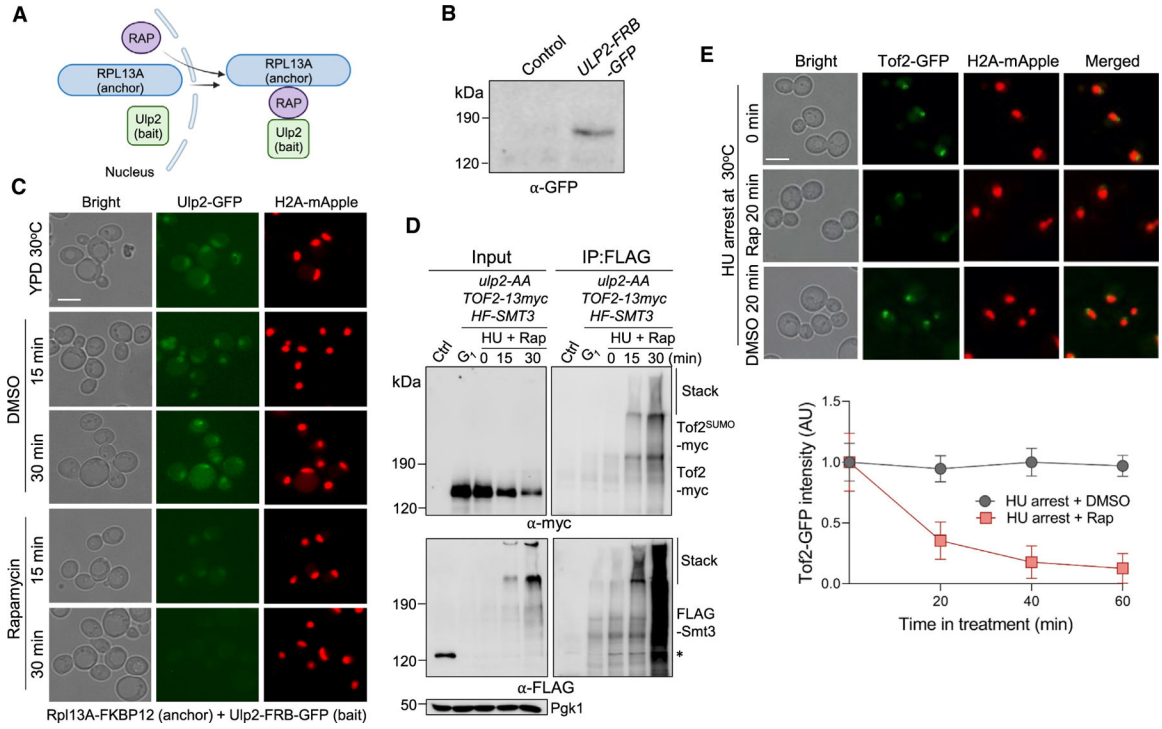

Figure 4. Nuclear depletion of SUMO protease Ulp2 induces Tof2 polySUMOylation and nucleolar delocalization

(A) Scheme of the Ulp2 “anchor away” system. The anchor, ribosomal protein RPL13A, is fused to two copies of the human FK506 binding protein FKBP12, while the target protein (Ulp2) is fused to the FRB domain. Rapamycin forms the RPL13A-rapamycin-Ulp2 complex, moving it to the cytoplasm and depleting Ulp2 from the nucleus.

(B) Expression of Ulp2-FRB-GFP in the constructed *ulp2-AA* strain. Shown is detection of Ulp2-FRB-GFP expression by western blotting in control (RTY3185) and *ulp2-AA* (4338-5-4) cells.

(C) *ulp2-AA* cells show rapid Ulp2 nuclear depletion upon rapamycin addition. Asynchronous *ulp2-AA* (4372-14-1) cells expressing bait Ulp2-FRB-GFP and anchor Rpl13A-23FKBP12 were treated with 2 μg/mL rapamycin or vehicle control DMSO and examined for Ulp2-FRB-GFP signal. H2A-mApple, nuclear marker. Scale bar, 5 μm.

(D) Nuclear depletion of Ulp2 in *ulp2-AA* cells triggers Tof2 polySUMOylation and degradation. Log-phase *ulp2-AA* cells expressing Tof2-13myc and HF-Smt3 (4442-3-1) were either arrested with α-factor or HU for 2 h. HU-arrested cells were subjected to rapamycin treatment. Cell extracts were IPed to isolate HF-Smt3 conjugates. HF-Smt3 and Tof2-13myc protein levels in the input and IPed fraction were detected by western blotting. Y300 (WT) cells served as a negative control. Pgk1, loading control.

(E) Tof2-GFP delocalizes from the nucleolus upon nuclear depletion of Ulp2. *ulp2-AA TOF2-GFP* (4374-4-2) cells were arrested with HU. Then, rapamycin or DMSO was added, and cells were collected for imaging. The average Tof2-GFP intensity for each time point (n = 50 cells) was quantified. The line graph represents mean values ± SD. H2A-mApple, nuclear marker. Scale bar, 5 mm.

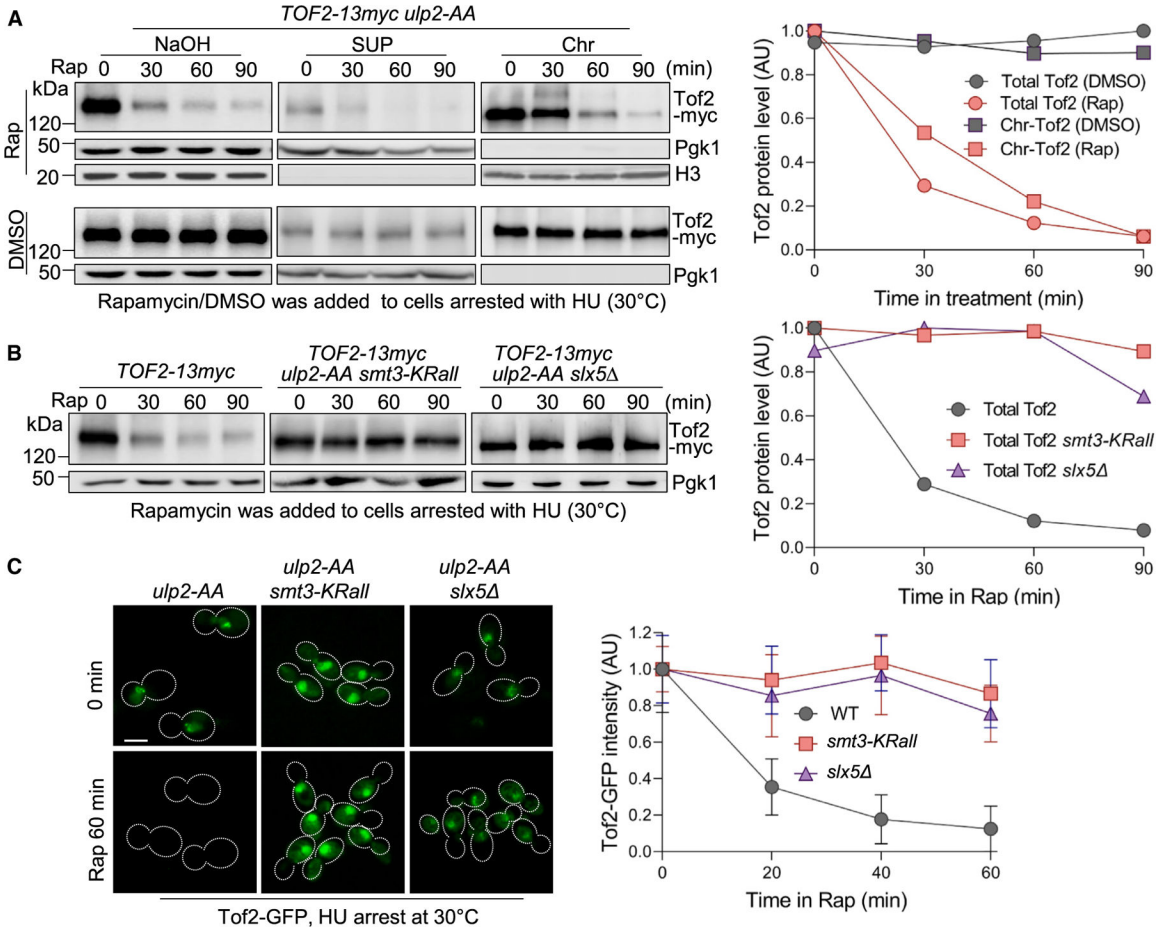

Figure 5. Block of polySUMOylation or deletion of STUbL gene *SLX5* suppresses Tof2 delocalization and degradation

(A) Nuclear depletion of Ulp2 in *ulp2-AA* cells triggers chromatin dissociation and turnover of Tof2. *ulp2-AA TOF2–13myc* (4366-14-1) cells were first arrested with HU. After rapamycin addition, cells were collected for chromatin fractionation (STAR Methods). Tof2-13myc protein levels were detected by western blotting. Pgk1, cytoplasmic protein control. Histone H3, chromatin-bound protein control. Tof2 protein levels were normalized by determining the ratio to Pgk1. Chr, chromatin; SUP, supernatant.

(B) The *smt3-KRall* or *slx5Δ* mutant stabilizes Tof2 in *ulp2-AA* cells after Ulp2 depletion. *ulp2-AA* (4366-14-1), *ulp2-AA smt3-KRall* (4422-3-2), and *ulp2-AA slx5Δ* (4389-13-1) cells containing Tof2-13myc were first arrested with HU. After rapamycin addition, cells were collected over time. Tof2-13myc protein levels were detected by western blotting. Pgk1, loading control. Total Tof2 protein levels were quantified as described in (A).

(C) The *smt3-KRall* or *slx5Δ* mutant prevents nucleolar delocalization of Tof2-GFP induced by Ulp2 depletion. *ulp2-AA* (4374-4-2), *ulp2-AA smt3-KRall* (4451-3-3), and *ulp2-AA slx5Δ* (4453-1-4) cells containing Tof2-GFP were arrested with HU, and then rapamycin was added. Cells were fixed before imaging. Representative images are shown on the left. The average Tof2-GFP intensity for each time point (n = 50 cells) was quantified. The line graph represents mean values ± SD. Scale bar, 5 μm.

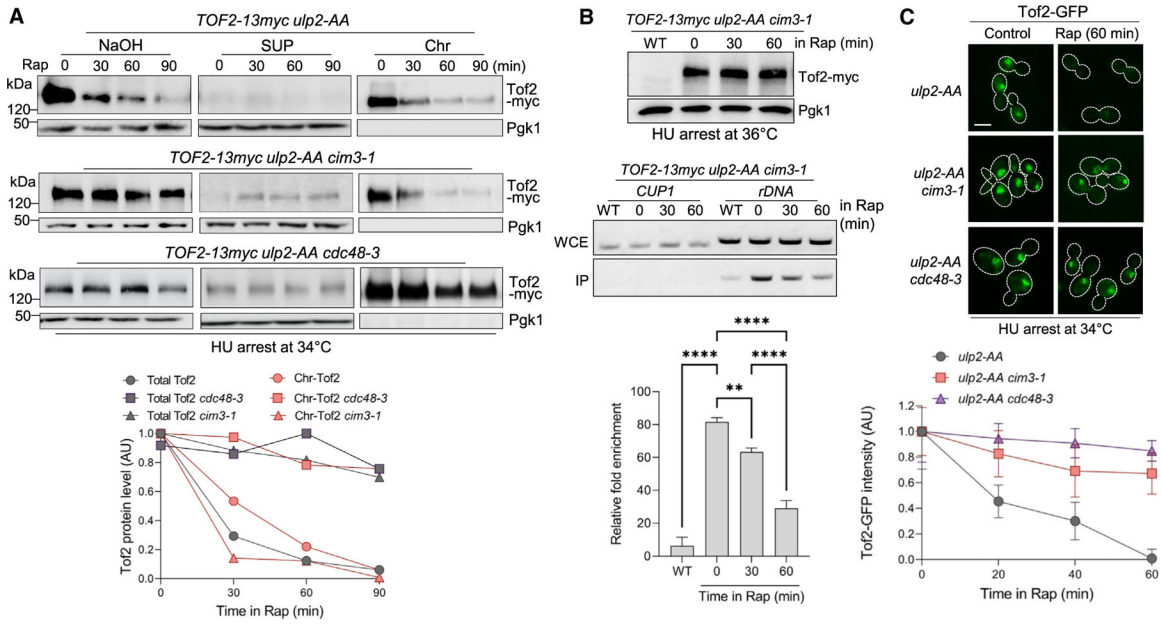

Figure 6. The role of Cdc48 segregase and the proteasome in polySUMO-induced chromatin dissociation and degradation of Tof2

(A) Tof2 degradation and chromatin binding in cells with compromised activity of segregase (*cdc48-3*) and the proteasome (*cim3-1*). *ulp2-AA* (4366-14-1), *ulp2-AA cdc48-3* (4381-2-1), and *ulp2-AA cim3-1* (4414-5-4) cells containing Tof2-13myc at 25°C were arrested with HU and then shifted to 34°C for 2 h before rapamycin treatment. Cells were collected for chromatin fractionation (STAR Methods). Tof2-13myc protein levels were detected by western blotting. Pgk1, control for cytoplasmic proteins. Tof2 protein levels were normalized by determining the ratio to Pgk1.

(B) Tof2 dissociates from rDNA upon polySUMOylation induction. ChIP was performed with anti-Myc antibody using untagged control (Y300/WT) and *ulp2-AA cim3-1 TOF2-13myc* (4414-5-4) cells. Tof2-associated DNA was determined by PCR with primers specific for rDNA or *CUP1* (see STAR Methods for details). The relative fold enrichment at rDNA was calculated from three repeats. Statistical analysis used one-way ANOVA with Tukey's test.

(C) Nucleolar localization of Tof2-GFP in *cdc48-3* or *cim3-1* mutants after Ulp2 nuclear depletion. *ulp2-AA* (4374-4-2), *ulp2-AA cdc48-3* (4451-3-3), and *ulp2-AA cim3-1* (4453-1-4) cells at 25°C were arrested with HU and then shifted to 34°C for 2 h. After rapamycin addition, cells were collected and fixed for imaging. The average Tof2-GFP intensity for each time point (n = 50 cells) was quantified. The line graph represents mean values ± SD. Scale bar, 5 μm.

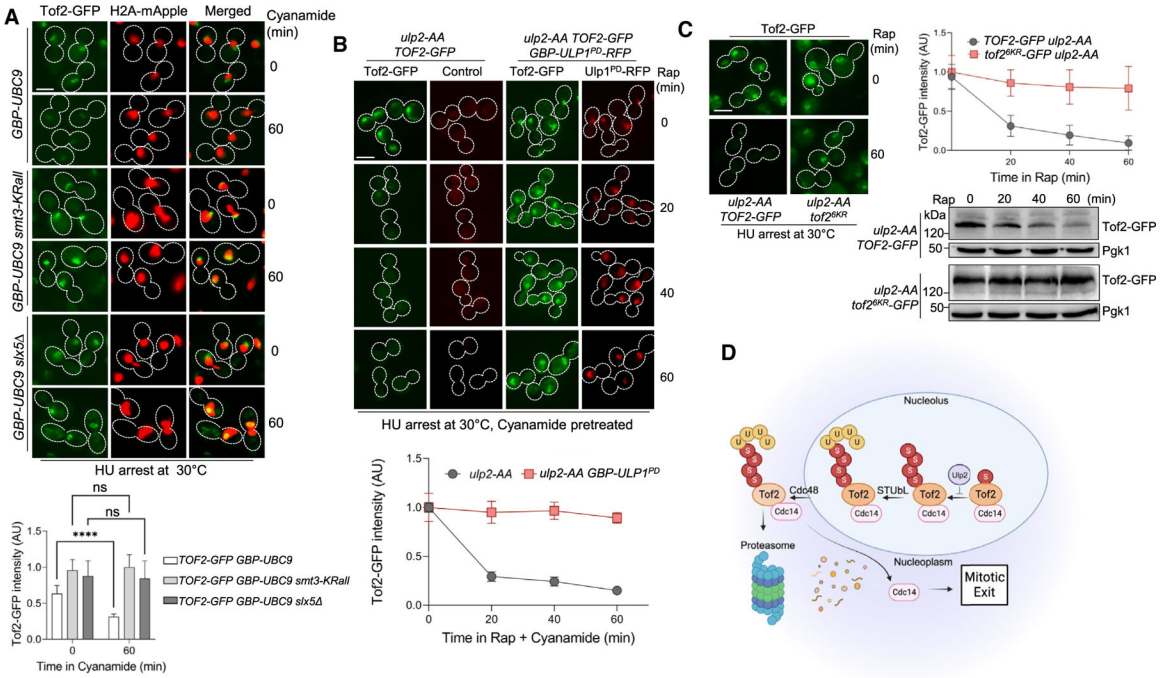

Figure 7. Tethering SUMO machinery to Tof2 is sufficient to alter its nucleolar localization and stability

(A) Tethering SUMO E2 enzyme Ubc9 to Tof2-GFP promotes its nucleolar delocalization through the polySUMO-dependent axis. *TOF2-GFP* (EGM31), *TOF2-GFP smt3-KRall* (EGM32), and *TOF2-GFP slx5Δ* (EGM33) cells were arrested with HU, and then cyanamide was added to induce GBP-Ubc9 expression. Cells were collected at the indicated time points and fixed for imaging. The Tof2-GFP signal in representative cells is shown. H2A-mApple, nuclear marker. Scale bar, 5 μm. The average Tof2-GFP intensity for each time point (n = 50 cells) was quantified. Statistical analysis used two-way ANOVA with Tukey's test. Bar graph represents mean values ±SD.

(B) Tethering the SUMO protease domain of Ulp1 (Ulp1^{PD}) to Tof2-GFP prevents its nucleolar delocalization induced by nuclear Ulp2 depletion. *TOF2-GFP ulp2-AA* (4453-4-3) and *TOF2-GFP ulp2-AA* P_{DDI2}*HA-GBP-ULP1*^{PD}*-RFP* (4453-5-1) cells were arrested with HU, and then cyanamide was added to induce GBP-Ulp1^{PD} expression. After rapamycin addition, cells were collected and fixed for imaging. Tof2-GFP and GBP-Ulp1^{PD}-RFP in representative cells are shown. Scale bar, 5 μm. The average Tof2-GFP intensity for each time point (n = 50 cells) was quantified. The line graph represents mean values ± SD.

(C) PolySUMO-dependent Tof2 delocalization and degradation is blocked in the *tof2*^{6KR} mutant. *ulp2-AA TOF2-GFP* (EGM49) and *ulp2-AA tof2*^{6KR} (EGM50) cells were first arrested with HU and then treated with rapamycin. Tof2-GFP intensity and protein levels were examined. Scale bar, 5 μm. Pgk1, loading control. The average Tof2-GFP intensity for each time point (n = 50 cells) was quantified. The line graph represents mean values ± SD.

(D) PolySUMO-dependent Tof2 nucleolar release and turnover drive mitotic exit. Ulp2 inactivation leads to Tof2 polySUMOylation, followed by STUbL-mediated ubiquitination and Cdc48-driven extraction. This axis enables Tof2 nucleolar release and proteasomal degradation, triggering Cdc14 release and mitotic exit.

KEY RESOURCES TABLE

REAGENT or RESOURCE	SOURCE	IDENTIFIER
Antibodies		
Mouse monoclonal anti-FLAG	Sigma Aldrich	Cat# F3165; RRID:AB_259529
Mouse monoclonal anti-Pgk1+	Invitrogen	Cat# 459250; RRID:AB_2532235
Mouse monoclonal anti-HA	Biolegend	Cat# 901515; RRID:AB_2565334
Mouse monoclonal anti-c-Myc	Biolegend	Cat# 626801; RRID:AB_2235686
Mouse monoclonal anti-Smt3	Santa Cruz	Cat# SC-137158; RRID:AB_201891
Mouse anti-FLAG M2 (agarose beads) affinity gel	Sigma	Cat# A2220; RRID:AB_10063035
Protein A/G PLUS-Agarose	Santa Cruz	Cat#SC-2003; RRID:AB_10201400
Mouse anti-GFP antibody	Santa Cruz	Cat# Sc-9966; RRID:AB_627235
Secondary anti-mouse IgG HRP-linked antibody	Cell Signaling	Cat# 7076; RRID:AB_330924
Rabbit monoclonal anti-histone H3	Millipore Sigma	Cat# 04–928; RRID:AB_10564360
IRDye® 680RD goat anti-rabbit IgG secondary antibody	Li-Cor	Cat#926–68073; RRID:AB_10954442
Chemicals, peptides, and recombinant proteins		
MG132	Sigma-Aldrich	474790
Protease inhibitor cocktail set III	Millipore-Calbiochem	539136
DeSUMOylation inhibitor N-ethylmaleimide	Sigma-Aldrich	E3876
ECL	PerkinElmer	NEL 104001
Hydroxyurea	Ambeed	A145474
Nocodazole	Sigma	M1404
Rapamycin	Thermo-Scientific	PHZ1235
Cyanamide	BeanTown Chemical	420-04-2
Critical commercial assays		
E.Z.N.A.® Gel Extraction Kit	Omega Bio-tek	Cat# D2500-01
E-Z 96™ Cycle Pure Kit	Omega Bio-tek	Cat# D1043
E.Z.N.A.® Plasmid DNA Mini Kit II	Omega Bio-tek	Cat# D6945-01
Deposited data		
Raw data	This paper; Mendeley	https://doi.org/10.17632/cbnt5zkgf3.1
Experimental models: organisms/strains		
S. cerevisiae: strain background W303; see Table S1	This paper	N/A
Software and algorithms		
ImageJ	National Institutes of Health	https://imagej.nih.gov/ij/
GraphPad Prism	Dotmatics	https://www.graphpad.com/